Bayesian inversion using adaptive Polynomial Chaos Kriging within Subset Simulation

D. Rossat, J. Baroth, Matthieu Briffaut, F. Dufour

Version of Record: https://www.sciencedirect.com/science/article/pii/S0021999122000481
Manuscript_15e65ba76ce2d77bcdcecf5b543fc737

Bayesian inversion using adaptive Polynomial Chaos Kriging within Subset Simulation

D. Rossat[a,b,*], J. Baroth[a], M. Briffaut[a], F. Dufour[a]

[a] *Univ. Grenoble Alpes, CNRS, Grenoble INP, 3SR, F-38000 Grenoble, France*

[b] *Electricité de France (EDF-DIPNN-DT), 69007 Lyon, France*

Abstract

In this paper, we propose a Bayesian inversion approach combining adaptive *Polynomial Chaos Kriging* (PCK) surrogate models and a rare event estimation method called *Subset Simulation* (SuS). It is based on the recently introduced *Bayesian Updating with Structural reliability* (BUS) framework that enables to reformulate the classical Bayesian inference into a rare event estimation problem. In this context, the SuS method aims at drawing samples from the posterior distribution as well as estimating the model evidence, which is usually computationally intractable when considering classical MCMC approaches. The proposed approach involves the construction of a PCK surrogate model which provides both global and local approximations of the likelihood function, through the combination of a Polynomial Chaos and Kriging surrogates. Furthermore, we propose an adaptive scheme for enriching the PCK surrogate throughout the SuS sampling procedure, in order to improve its accuracy near informative regions. The applicability and the efficiency of the proposed approach are assessed through its application to three cases studies with increasing complexity. Results highlighted that the proposed approach enables to accurately approximating posteriors with a limited amount of full model calls, even in the case of multi-modal posteriors, which are usually difficult to sample when using classical MCMC algorithms.

Keywords: , Bayesian inversion, Polynomial Chaos, Kriging, Structural Reliability Methods, Subset Simulation, Inverse problems

*Corresponding author
Email address: donatien.rossat@3sr-grenoble.fr (D. Rossat)

1. Introduction

In science and engineering, computational models are widely used for assessing the response of a physical system. Such models can be seen as input-output maps, which predict measurable quantities related to the system response for a given set of input parameters. Inverse problems consist of inferring these parameters given a set of observations of the system response [1].

In most cases, solving inverse problems remains a challenging task due to their *ill-posedness* in the Hadamard sense: indeed, a solution may not exist and/or be not unique, and may not be continuously varying with respect to the observation data. In this context, the Bayesian formulation for inverse problems provides a general framework for quantifying epistemic uncertainties on parameters, and assimilating noisy observation data in order to update these uncertainties. Based on probability theory, it requires the definition of a *prior* distribution which represents the beliefs before collecting observation data, and contributes to the regularization of ill-posed inverse problems [2, 3]. A discrepancy model is also required in order to link model predictions to observations, through the definition of a so-called *likelihood function*. Then, Bayesian inference provides a *posterior* distribution which summarizes all the available knowledge on parameters once the observation data have been collected and analyzed. This posterior distribution may subsequently be used for computing some Quantities of Interest (QoI) related to parameters, such as mean or covariance matrix, or marginals distributions. It is also possible to make new predictions by integrating over the posterior. Furthermore, the so-called *model evidence*, given by the normalization constant of the posterior, may be used for quantifying the plausibility of a given model given the available data, in the framework of model selection [4].

The computation of the posterior constitutes a major task of Bayesian inference. In general, a closed-form expression is not available, notably due to the fact that the model evidence is often a multi-dimensional integral, the calculation of which is often intractable. Then, the posterior is usually estimated from samples, and Monte Carlo estimates are often considered for computing posterior QoI. In this context, Markov Chain Monte Carlo (MCMC) techniques constitute a widely used class in the framework of Bayesian computations [5, 6]. They typically consist of generating Markov chains in the parameter space to draw samples from the posterior distribution, by avoiding the computation of the model evidence. In this context, the Metropolis-Hastings (MH) [7, 8] constitutes the cornerstone of MCMC algorithms. A wide range of MCMC variants have been developed, including adaptive variants [9, 10], algorithms based on Hamiltonian dynamics [11], or affine-invariant algorithms [12]. Nevertheless, MCMC algorithms suffer from several drawbacks: firstly, the Markovian nature of such processes induces sample auto-correlation, which may alter the reliability of Monte Carlo estimates of posterior QoI. Secondly, the absence of clear convergence criterion constitutes a major drawback. Instead, numerical heuristic criterion have been proposed in the literature [13, 14, 15]. Lastly, MCMC algorithms require a large amount of likelihood evaluations, which make such algorithms intractable when dealing with computationally extensive models.

Then, few alternatives to MCMC-based approaches have been proposed in the literature, such as Variational

Bayesian (VB) inference [16] aiming at computing the posterior by solving an optimization problem, Approximate Bayesian Computation (ABC) [17], Laplace approximations [18] or Nested Sampling [19, 20]. Recently, some authors have proposed novel *sampling-free* approaches, in the sense that an analytical form of the posterior is computed instead of drawing samples for estimating it. El Moselhy & Marzouk [21] introduced an approach based on optimal transport maps, which push forward the prior to the posterior. Nagel & Sudret [22] introduced the so-called Spectral Likelihood Expansion (SLE) approach, based on a spectral representation of the likelihood function in a basis of polynomials which are orthonormal with respect to the prior. Then, as a generalization of SLE, Wagner et al. [23] proposed an adaptive approach based on Stochastic Spectral Embedding (SSE) [24], which aims at constructing local spectral expansions of the likelihood function.

Another recent novel framework for Bayesian computations has been introduced by Straub & Papaionannou [25], known as Bayesian Updating with Structural reliability methods (BUS). It aims at reformulating the classical Bayesian inference formulation into a rare event estimation problem [26]. Structural Reliability (SR) methods [27, 28] have been developed in order to estimate the probability of rare events, based on physical and engineering models. Then, such methods can be used in the BUS framework, in order to compute the posterior as well as the model evidence, since the latter can be written as the probability of a rare event [26]. In particular, the Subset Simulation (SuS) method [29] constitutes a widely used SR method, enabling to estimate the probability of rare events for a wide range of applications. Such method has been recently implemented in the BUS framework [30], in order to efficiently draw samples from posterior distributions.

Nevertheless, such approach requires an important amount of likelihood evaluations, as MCMC sampling techniques. Firstly, some authors proposed to accelerate MCMC calculations by using surrogate models. In this context, surrogates may be constructed offline, and then used for replacing the full forward model throughout MCMC sampling. Such strategy has been considered with Polynomial Chaos (PC) surrogates based on the prior distribution [31, 32, 33], or with Kriging surrogates [34]. Another approach consists in adaptively refining the surrogate model throughout the sampling procedure, as proposed in [35] for PC surrogates or in [36] for Deep Neural Networks (DNN), to name a few. Likewise, in the BUS framework, some authors recently proposed approaches based on surrogate models: Giovanis et al. [37] proposed an approach based on SuS and Artificial Neural Networks (ANN), whereas Wang & Shafieezadeh [38] combined adaptive Kriging and Rejection Sampling (RS).

Moreover, SR methods provide a wide range of active learning approaches, enabling to construct surrogate models with adaptive experimental designs, which are iteratively enriched to improve the accuracy of surrogate model predictions of QoI related to rare events [39, 40]. In particular, such approaches tend to limit the number of model calls, which makes their use suitable for computationally expensive models. In this context, *local* surrogate models such as Kriging [41, 38] are often considered, due to the local error measure they provide, which can be used for selecting new enrichment points for experimental designs. Recently, Schöbi et al. [42] proposed a new surrogate modeling technique named Polynomial Chaos Kriging (PCK), which combines a PC for approximating the global behavior of the model, and a Kriging for catching local variations. PCK provides

Kriging local features (*e.g.* prediction variance) to a PC surrogate, by embedding a PC into the trend of a Kriging process. Hence, PCK surrogate models are well suited for Kriging-based active learning approaches, which makes it a powerful candidate for rare event estimation, as highlighted in [43].

In this paper, a hybrid Bayesian inversion approach based on the BUS framework is proposed, which uses adaptive PCK surrogate models within SuS. In this context, our main contributions are the following:

- We propose an implementation of PCK within SuS in the BUS framework, to accelerate the SuS sampling procedure. The main idea is to construct a PCK surrogate of the log-likelihood function, which can be enriched in an adaptive way throughout the rare event estimation procedure performed with SuS.
- In order to improve the accuracy of the PCK in posterior high-probability zones with a limited number of full model calls, we propose an active learning scheme for adaptively refining the PCK surrogate in posterior high-probability zones.

Firstly, a global approximation of the log-likelihood on the prior support is constructed, by using an Experimental Design (ED) of limited size. It is well known that the accuracy of prior-based surrogates near posterior high-probability zones cannot be guaranteed in general [44, 35]. This motivates the introduction of the proposed active learning scheme: the ED of the PCK is then iteratively enriched by selecting points in *informative* zones, based on a combination of PCK local features and a clustering technique [45]. The proposed approach enables to efficiently improve the local accuracy of the PCK surrogate with a limited amount of full model calls. More specifically, such adaptive scheme enables to handle multi-modal posteriors, which are difficult to sample when using classical MCMC sampling approaches. The approach fully exploits the versatility of PCK, by firstly capturing the global trend of the posterior and subsequently focusing on informative zones.

The paper is organized as follows: the basics of Bayesian inference and the BUS framework are briefly presented in Section 2. Then, Section 3 establishes the main theoretical and practical basics related to PCK surrogate models. The proposed Bayesian inversion approach is subsequently described in Section 4. The performance of the proposed approach is assessed in Section 5, through four cases studies of increasing complexity. Lastly, the paper is summarized and concluded in Section 6.

2. Bayesian Updating with Structural reliability methods (BUS)

2.1. Bayesian inference

Let $(\Omega, \mathcal{F}, \mathbb{P})$ be a probability space, where Ω is a sample space, $\mathcal{F}$ a Borel algebra on Ω and $\mathbb{P}$ a probability measure on $(\Omega, \mathcal{F})$. Consider a system with uncertain parameters, which are represented by a random vector $\boldsymbol{\Theta} : \Omega \longrightarrow \mathcal{D}_{\boldsymbol{\theta}} \subset \mathbb{R}^m$. The behavior of the system is represented by an computational model $\mathcal{M} : \mathcal{D}_{\boldsymbol{\theta}} \longrightarrow \mathcal{D}_{\boldsymbol{y}} \subset \mathbb{R}^n$ which maps a set of parameters $\boldsymbol{\theta} \in \mathcal{D}_{\boldsymbol{\theta}}$ to a response $\mathcal{M}(\boldsymbol{\theta})$. The random vector $\boldsymbol{\Theta}$ is assumed to admit a

Probability Density Function (PDF) denoted by $\rho(\boldsymbol{\theta})$, which expresses the prior belief in $\boldsymbol{\Theta}$. Then, let suppose that a set of observations of the system response is available, and gathered in a vector $\boldsymbol{y} \in \mathcal{D}_{\boldsymbol{y}}$. The so-called *likelihood function* $\mathcal{L}(\boldsymbol{\theta}; \boldsymbol{y})$ is proportional to the probability of observing $\boldsymbol{y}$ given a realization $\boldsymbol{\Theta} = \boldsymbol{\theta}$ of the uncertain parameters. In order to link observations to responses of $\mathcal{M}$, an additive Gaussian discrepancy model is often considered:

$$\boldsymbol{y} = \mathcal{M}(\boldsymbol{\theta}) + \boldsymbol{\varepsilon} \tag{2.1}$$

where $\boldsymbol{\varepsilon} \sim \mathcal{N}_n(\mathbf{0}, \boldsymbol{\Sigma}_{\boldsymbol{\varepsilon}})$ is a normal random vector with zero mean and covariance matrix $\boldsymbol{\Sigma}_{\boldsymbol{\varepsilon}}$. In this case, the likelihood function reads:

$$\mathcal{L}(\boldsymbol{\theta}; \boldsymbol{y}) = \phi_n(\boldsymbol{y} - \mathcal{M}(\boldsymbol{\theta}); \boldsymbol{\Sigma}_{\boldsymbol{\varepsilon}}) \tag{2.2}$$

where $\phi_n(\cdot; \boldsymbol{\Sigma}_{\boldsymbol{\varepsilon}})$ is the PDF of the distribution $\mathcal{N}_n(\mathbf{0}, \boldsymbol{\Sigma}_{\boldsymbol{\varepsilon}})$.

Then, applying Bayes' theorem, the *posterior* PDF $\pi(\boldsymbol{\theta}|\boldsymbol{y})$ of $\boldsymbol{\Theta}$ can be written as follows:

$$\pi(\boldsymbol{\theta}|\boldsymbol{y}) = \frac{\rho(\boldsymbol{\theta})\mathcal{L}(\boldsymbol{\theta}; \boldsymbol{y})}{\mathcal{Z}} \tag{2.3}$$

where $\mathcal{Z}$ is a normalization constant, known as *model evidence*:

$$\mathcal{Z} = \int_{\mathcal{D}_{\boldsymbol{\theta}}} \rho(\boldsymbol{\theta})\mathcal{L}(\boldsymbol{\theta}; \boldsymbol{y}) \mathrm{d}\boldsymbol{\theta} \tag{2.4}$$

The posterior PDF (2.3) summarizes all available information on uncertain parameters $\boldsymbol{\Theta}$ after the data have been collected. In most cases, the posterior PDF does not admit a closed-form expression. Moreover, the model evidence is often a multidimensional integral which is computationally expensive to evaluate. In this context, Markov Chain Monte Carlo (MCMC) methods are widely used for drawing samples from the posterior distribution, without computing the model evidence [5, 6]. Such methods aim at constructing an ergodic Markov chain $\left(\boldsymbol{\Theta}^{(\tau)}\right)_{\tau \in \mathbb{N}}$ whose invariant distribution is the posterior distribution, which writes:

$$\pi(\boldsymbol{\theta}^{(\tau+1)}|\boldsymbol{y}) = \int_{\mathcal{D}_{\boldsymbol{\theta}}} \pi(\boldsymbol{\theta}^{(\tau)}|\boldsymbol{y}) \mathcal{K}(\boldsymbol{\theta}^{(\tau)}, \boldsymbol{\theta}^{(\tau+1)}) \mathrm{d}\boldsymbol{\theta}^{(\tau)} \tag{2.5}$$

where $\mathcal{K}(\boldsymbol{\theta}, \boldsymbol{\theta}')$ is the density of the transitional distribution from the state $\boldsymbol{\theta}^{(\tau)}$ of the chain $\left(\boldsymbol{\Theta}^{(\tau)}\right)_{\tau \in \mathbb{N}}$ to the state $\boldsymbol{\theta}^{(\tau+1)}$. A sufficient condition for Eq.(2.5) to apply is the so-called *detailed balance* condition, which expresses the time-reversibility of the Markov chain:

$$\pi(\boldsymbol{\theta}^{(\tau)}|\boldsymbol{y}) \mathcal{K}(\boldsymbol{\theta}^{(\tau)}, \boldsymbol{\theta}^{(\tau+1)}) = \pi(\boldsymbol{\theta}^{(\tau+1)}|\boldsymbol{y}) \mathcal{K}(\boldsymbol{\theta}^{(\tau+1)}, \boldsymbol{\theta}^{(\tau)}) \tag{2.6}$$

This condition is generally verified for most MCMC algorithms, such as the well-known Metropolis-Hastings algorithm [7, 8], which constitutes the cornerstone of MCMC.

2.2. The BUS framework

2.2.1. Structural Reliability problems

The BUS framework, initially introduced in [25], consists in reformulating the classical Bayesian updating problem presented in Section 2.1 into a Structural Reliability (SR) problem. SR methods aim at estimating the probability of rare events [27, 46]. Such events are usually described in terms of a *limit state function* (LSF) $h : \mathcal{D}_{\boldsymbol{x}} \longrightarrow \mathbb{R}$, whose values are classifying *safety* and *failure* domains D_s, D_f respectively, in the space $\mathcal{D}_{\boldsymbol{x}}$ of the random parameters $\boldsymbol{X}$ of the reliability problem:

$$\begin{aligned} D_s &= \{\boldsymbol{x} \in \mathcal{D}_{\boldsymbol{x}} \mid h(\boldsymbol{x}) > 0\} \\ D_f &= \{\boldsymbol{x} \in \mathcal{D}_{\boldsymbol{x}} \mid h(\boldsymbol{x}) \leq 0\} \end{aligned} \tag{2.7}$$

The main goal of SR methods is to estimate the failure probability $\mathbb{P}_f = \mathbb{P}(h(\boldsymbol{X}) \in D_f)$, which can be written as the following integral if $\boldsymbol{X}$ admits a density $\rho(\boldsymbol{x})$:

$$\mathbb{P}_f = \int_{\mathcal{D}_{\boldsymbol{x}}} \mathbf{1}_{D_f}(\boldsymbol{x}) \rho(\boldsymbol{x}) \mathrm{d}\boldsymbol{x} \tag{2.8}$$

where $\mathbf{1}_A$ is the indicator function of $A \subset \mathcal{D}_{\boldsymbol{x}}$.

The integral which defines the probability (2.8) can not be solved analytically in the general case. The Rejection Sampling (RS) method aims at estimating $\mathbb{P}_f$ by Monte Carlo simulation:

$$\widehat{\mathbb{P}}_f = \frac{1}{N} \sum_{n=1}^{N} \mathbf{1}_{\mathcal{D}_f}(\boldsymbol{x}^{(n)}) \tag{2.9}$$

where $(\boldsymbol{x}^{(1)}, \ldots, \boldsymbol{x}^{(N)})$ are samples drawn from the distribution of the parameters $\boldsymbol{X}$. The accuracy of this estimate may be measured by computing the Coefficient of Variation (CoV) of $\widehat{\mathbb{P}}_f$, which is given by:

$$\mathbf{CoV}\left[\widehat{\mathbb{P}}_f\right] = \sqrt{\frac{1 - \widehat{\mathbb{P}}_f}{N \widehat{\mathbb{P}}_f}} \tag{2.10}$$

It appears from Eq. (2.10) that such direct Monte Carlo estimation may become inefficient when failure probabilities are small. Indeed, the required number of samples to obtain a target CoV dramatically increases when the failure probability is decreasing.

In this context, several alternative SR methods have been developed in order to provide more efficient estimations of failure probabilities, such as First Order Reliability Method (FORM) [28], importance sampling [47], or Subset Simulation (SuS) [29]. One will focus on the latter method in the present paper.

2.2.2. BUS framework formulation

Keeping the notations introduced in Section 2.1, let $p : \Omega \longrightarrow \mathcal{D}_p = [0,1]$ a random variable uniformly distributed on $[0,1]$ (*i.e.* $p \sim \mathcal{U}([0,1])$), which is assumed to be independent from the parameters $\boldsymbol{\Theta}$. The BUS framework proposes to consider the parameters $(\boldsymbol{\Theta}, p)$ which take values in the augmented space $\mathcal{D}_{\boldsymbol{\theta}} \times \mathcal{D}_p$, as well as the failure event $F \subset \mathcal{D}_{\boldsymbol{\theta}} \times \mathcal{D}_p$ defined by:

$$F = \{(\boldsymbol{\theta}, p) \in \mathcal{D}_{\boldsymbol{\theta}} \times \mathcal{D}_p \mid p \leq c\mathcal{L}(\boldsymbol{\theta}; \boldsymbol{y})\} \tag{2.11}$$

where $c > 0$ is a constant, chosen such that $c\mathcal{L}(\boldsymbol{\theta}; \boldsymbol{y}) \leq 1, \ \forall \boldsymbol{\theta} \in \mathcal{D}_{\boldsymbol{\theta}}$. The choice of such constant will be detailed in further sections.

It has been demonstrated in [25] that the posterior PDF $\pi(\boldsymbol{\theta}|\boldsymbol{y})$ given in Eq. (2.3) rewrites as follows:

$$\pi(\boldsymbol{\theta}|\boldsymbol{y}) = \frac{1}{\mathbb{P}_f} \int_{\mathcal{D}_p} \mathbf{1}_F(\boldsymbol{\theta}, p)\rho(\boldsymbol{\theta})\mathrm{d}p \tag{2.12}$$

where $\mathbb{P}_f$ is the failure probability given by:

$$\mathbb{P}_f = \mathbb{P}((\boldsymbol{\Theta}, p) \in F) = \int_{\mathcal{D}_{\boldsymbol{\theta}}} \int_{\mathcal{D}_p} \mathbf{1}_F(\boldsymbol{\theta}, p)\rho(\boldsymbol{\theta})\mathrm{d}p\mathrm{d}\boldsymbol{\theta} \tag{2.13}$$

Thus, Eqs. (2.12) and (2.13) ensure that sampling from the posterior distribution is tantamount to solving the reliability problem in the augmented space $\mathcal{D}_{\boldsymbol{\theta}} \times \mathcal{D}_p$ with the LSF given by [25]:

$$h(\boldsymbol{\theta}, p) = p - c\mathcal{L}(\boldsymbol{\theta}; \boldsymbol{y}) \tag{2.14}$$

Moreover, it is worth noting that the failure probability $\mathbb{P}_f$ is directly linked to the model evidence given by Eq. (2.4). Indeed, rewriting the integral in Eq. (2.13) yields:

$$\mathbb{P}_f = c \int_{\mathcal{D}_{\boldsymbol{\theta}}} \mathcal{L}(\boldsymbol{\theta}; \boldsymbol{y})\rho(\boldsymbol{\theta})\mathrm{d}\boldsymbol{\theta} = c\mathcal{Z} \tag{2.15}$$

2.3. BUS and subset simulation

2.3.1. Formulation

Subset Simulation (SuS) [29] is a widely used SR method which enables to efficiently estimate small failure probabilities in high-dimensional random variable spaces. The main idea of SuS consists in expressing the rare event F in Eq. (2.11) as an intersection of nested intermediate events $F_r \subset \cdots \subset F_1 \subset F_0$, where F_0 is the certain event (*i.e.* $\mathbb{P}(F_0) = 1$) and $F_r = F$. In this framework, the failure probability in Eq. (2.13) rewrites:

$$\mathbb{P}_f = \mathbb{P}\left(\bigcap_{i=0}^{r} F_i\right) = \prod_{i=1}^{r} \mathbb{P}(F_i|F_{i-1}) \tag{2.16}$$

Thus, the failure probability $\mathbb{P}_f$ is expressed as a product of larger conditional probabilities, which can be more efficiently estimated than a single small probability. Following [29] and [30], the intermediate events are defined by using a sequence of threshold values $0 = h_r < \cdots < h_1 < h_0 = +\infty$:

$$F_i = \{(\boldsymbol{\theta}, p) \in \mathcal{D}_{\boldsymbol{\theta}} \times \mathcal{D}_p \mid h_l(\boldsymbol{\theta}, p) \leq h_i\} \tag{2.17}$$

where $h_l(\boldsymbol{\theta}, p)$ is a modified form of the LSF function $h(\boldsymbol{\theta}, p)$ given by Eq. (2.14):

$$h_l(\boldsymbol{\theta}, p) = \log(p) - \log(c) - \log(\mathcal{L}(\boldsymbol{\theta})) \tag{2.18}$$

where the dependence to data $\boldsymbol{y}$ of $\mathcal{L}$ will be omitted for the sake of concision.

Such LSF formulation has been introduced in [30] in order to ensure smooth transitions between intermediate events, and therefore to improve numerical stability of SuS within BUS [37].

The threshold values $(h_i)_{1 \leq i \leq r}$ are chosen so that the corresponding conditional probabilities $(\mathbb{P}(F_i|F_{i-1}))_{1 \leq i \leq r}$ are equal to a value $\mathbb{P}_t$ in average, usually chosen as $\mathbb{P}_t = 10\%$ [29, 48, 30]. In this way, the estimation of the probabilities $(\mathbb{P}(F_i|F_{i-1}))_{1 \leq i \leq r}$ through Monte Carlo estimation is sensibly more efficient than the direct estimation of $\mathbb{P}_f$. The generation of samples splits into two parts: firstly, samples are drawn from the prior distribution in order to estimate the probability $\mathbb{P}(F_1|F_0)$ through direct Monte Carlo (see Eq. (2.9)). Next, for each $i \in \{1, \ldots, r\}$, samples conditional to intermediate event F_i are generated with MCMC sampling, as described by Algorithm 1. Finally, samples of the last SuS level correspond to samples of the posterior distribution of parameters $\boldsymbol{\Theta}$. It is important to underline that the model evidence (see Eq. (2.4)) is available as a by-product of the SuS procedure, due to the relation given in Eq.(2.15). Then, unlike classical MCMC sampling methods which provide posterior samples by avoiding to compute the model evidence, the SuS procedure applied in the BUS framework enables to both draw posterior samples and compute the model evidence.

2.3.2. MCMC sampling within SuS

In this paper, MCMC sampling (Step 5 of Algorithm 1) will be performed by using the adaptive Conditional Sampling (aCS) algorithm introduced in [49]. The samples are generated in an underlying standard normal probability space, also known as U-space, by considering an isoprobabilistic transform $\mathcal{T} : \mathcal{D}_{\boldsymbol{\theta}} \times \mathcal{D}_p \longrightarrow \mathcal{D}_{\boldsymbol{u}} = \mathbb{R}^{m+1}$, which maps the random vector $(\boldsymbol{\Theta}, p)$ to a standard normal uncorrelated random vector $\boldsymbol{U}$. Such mapping can be performed by using the Nataf [50, 51] or Rosenblatt [52] transform. Then, considering a Markov chain state $\boldsymbol{u} \in \mathcal{D}_{\boldsymbol{u}}$, a candidate sample $\boldsymbol{v} \sim \mathcal{N}_{m+1}(\boldsymbol{u}, \mathbf{I})$ is drawn, by imposing that $\boldsymbol{u}$ and $\boldsymbol{v}$ are jointly Gaussian with component-wise cross-correlation coefficients equal to $\rho \in [0, 1]$. This correlation parameter is adapted on the fly through MCMC sampling, in order to obtain an optimal Markov chain acceptance rate. For further details, the reader is referred to [49].

Algorithm 1: Subset Simulation in the BUS framework [29, 30].

Input: Number of samples per subset K, probability of intermediate subsets $\mathbb{P}_t$, BUS normalizing constant c

Output: Samples $(\boldsymbol{\theta}^{(i,k)}, p^{(i,k)})_{(i,k)\in\{0,\dots,r\}\times\{1,\dots,K\}}$, failure probability $\mathbb{P}_f$

Initialization;

1. Draw K samples $(\boldsymbol{\theta}^{(0,k)}, p^{(0,k)})_{k\in\{1,\dots,K\}}$ from the prior distribution of $(\boldsymbol{\Theta}, p)$;
2. Set $i = 0$ and $p_0 = 1$;

while $h_i > 0$ **do**

3. Set $i = i + 1$;
4. Sort $(\boldsymbol{\theta}^{(i-1,k)}, p^{(i-1,k)})_{k\in\{1,\dots,K\}}$ with respect to the LSF values $(h_l(\boldsymbol{\theta}^{(i-1,k)}, p^{(i-1,k)}))_{k\in\{1,\dots,K\}}$;
4. Set h_i as the $\mathbb{P}_t$-percentile of the set $(\boldsymbol{\theta}^{(i-1,k)}, p^{(i-1,k)})_{k\in\{1,\dots,K\}}$ with respect to the LSF values $(h_l(\boldsymbol{\theta}^{(i-1,k)}, p^{(i-1,k)}))_{k\in\{1,\dots,K\}}$;

if $h_i < 0$ **then**

Set $h_i = 0$ and $\mathbb{P}_i = \frac{n}{K}$, where $n = \text{Card}\left\{k \in \{1,\dots,K\} \;\middle|\; h_l(\boldsymbol{\theta}^{(i-1,k)}, p^{(i-1,k)}) \leq \max(h_i, 0)\right\}$;

else

Set $\mathbb{P}_i = \mathbb{P}_t$;

end

5. Generate the samples $(\boldsymbol{\theta}^{(i,k)}, p^{(i,k)})_{k\in\{1,\dots,K\}}$ by using MCMC. n Markov chains of length K/n are generated from the seeds $(\boldsymbol{\theta}^{(i-1,k)}, p^{(i-1,k)})_{k\in\{1,\dots,n\}}$;

end

6. Set $r = i$ and $\mathbb{P}_f = \prod_{j=0}^{r} \mathbb{P}_j$;

2.3.3. Choosing the BUS normalizing constant

Lastly, the choice of the BUS normalizing constant c plays a crucial role in the generation of posterior samples with the SuS procedure. The choice $c^{-1} = \mathcal{L}_{\max} = \max_{\boldsymbol{\theta}\in\mathcal{D}_{\boldsymbol{\theta}}} \mathcal{L}(\boldsymbol{\theta})$ clearly constitutes the optimal choice. However, such value is not known in advance in general. Moreover, evaluating the likelihood function may require an important computational cost, which makes Maximum Likelihood Estimate (MLE) potentially intractable. On the one hand, if $c^{-1} \leq \mathcal{L}_{\max}$, samples produced by BUS do not follow the posterior distribution [25, 53]. On the other hand, if $c^{-1} \geq \mathcal{L}_{\max}$, the efficiency of the BUS procedure may be affected, since the failure probability in Eq. (2.13) is proportional to c.

In this context, adaptive approaches have been proposed [54, 30] in order to learn the constant c during the SuS procedure. More specifically, such approaches consist in taking c as the largest likelihood within the already generated samples, and updating it when larger likelihood values are computed.

3. Surrogate modeling

3.1. Polynomial Chaos

3.1.1. Formulation

Keeping the notations introduced in Section 2, one supposes that the computational model takes scalar values, *i.e.* $\mathcal{M} : \mathcal{D}_{\boldsymbol{\theta}} \longrightarrow \mathbb{R}$. The following can be easily extended to the case of vector valued models. Furthermore,

the random vector $\boldsymbol{\Theta} : \Omega \longrightarrow \mathcal{D}_{\boldsymbol{\theta}}$ is supposed to have independent components, denoted by $(\Theta_1, \ldots, \Theta_m)$. Polynomial Chaos formulations for dependent input random variables can be found in [55, 56]. The marginal parameter space associated to Θ_i will be denoted by $\mathcal{D}_{\theta_i}$, so that $\mathcal{D}_{\boldsymbol{\theta}} = \prod_{i=1}^m \mathcal{D}_{\theta_i}$.

The PDF ρ_i of each component Θ_i enables to define a Hilbert space, namely the space $\mathbb{L}^2(\rho_i)$ of functions defined on $\mathcal{D}_{\theta_i}$ which are square integrable with respect to ρ_i:

$$\mathbb{L}^2(\rho_i) = \left\{ \phi : \mathcal{D}_{\theta_i} \longrightarrow \mathbb{R} \;\middle|\; \mathbb{E}\left[\phi(\Theta_i)^2\right] = \int_{\mathcal{D}_{\theta_i}} \phi(\theta)^2 \rho_i(\theta_i) \mathrm{d}\theta_i < +\infty \right\} \tag{3.1}$$

This space is equipped with the following inner product:

$$\langle \phi | \psi \rangle_{\rho_i} = \int_{\mathcal{D}_{\theta_i}} \phi(\theta_i)\psi(\theta_i)\rho_i(\theta_i)\mathrm{d}\theta_i = \mathbb{E}\left[\phi(\Theta_i)\psi(\Theta_i)\right] \tag{3.2}$$

for all $\phi, \psi \in \mathbb{L}^2(\rho_i)$. Then, it is possible to construct a Hilbert basis of $\mathbb{L}^2(\rho_i)$ formed by univariate polynomials $(\psi_j^{(i)})_{j \in \mathbb{N}}$ which are orthonormal with respect to ρ_i [57, 58]. Such construction has been originally introduced for Gaussian random variables by Wiener in [59], and then generalized to other distributions in [58] and [60]. In general, it is possible to construct a Hilbert basis of polynomials for a given probability distribution, under some conditions precised in [61].

Moreover, let $\mathbb{L}^2(\rho)$ be the Hilbert space of functions defined on $\mathcal{D}_{\boldsymbol{\theta}}$ which are square integrable with respect to ρ. This space is equipped with the inner product defined by $\langle \Phi | \Psi \rangle_\rho = \int_{\mathcal{D}_{\boldsymbol{\theta}}} \Phi(\boldsymbol{\theta})\Psi(\boldsymbol{\theta})\rho(\boldsymbol{\theta})\mathrm{d}\boldsymbol{\theta} = \mathbb{E}\left[\Phi(\boldsymbol{\Theta})\Psi(\boldsymbol{\Theta})\right]$. Knowing that the components $(\Theta_1, \ldots, \Theta_m)$ are mutually independent, their joint PDF π can be expressed as the tensor product of the marginals PDF:

$$\rho(\boldsymbol{\theta}) = \prod_{i=1}^m \rho_i(\theta_i) \tag{3.3}$$

for all $\boldsymbol{\theta} = (\theta_1, \ldots, \theta_m) \in \mathcal{D}_{\boldsymbol{\theta}}$. This ensures that $\mathbb{L}^2(\pi)$ is isomorphic to the tensorial product of Hilbert spaces $(\mathbb{L}^2(\rho_i))_{1 \leq i \leq m}$:

$$\mathbb{L}^2(\rho) \cong \bigotimes_{i=1}^m \mathbb{L}^2(\rho_i) \tag{3.4}$$

Consequently, the following multivariate polynomials define a hilbertian basis of $\mathbb{L}^2(\rho)$:

$$\Psi_{\boldsymbol{\alpha}}(\boldsymbol{\theta}) = \prod_{i=1}^m \psi_{\alpha_i}^{(i)}(\theta_i) \tag{3.5}$$

where the multi-index notation $\boldsymbol{\alpha} = (\alpha_1, \ldots, \alpha_m) \in \mathbb{N}^m$ has been used. Such polynomials are orthonormal with respect to π (*i.e.* $\langle \Psi_{\boldsymbol{\alpha}} | \Psi_{\boldsymbol{\beta}} \rangle_\rho = \delta_{\boldsymbol{\alpha}\boldsymbol{\beta}}$, where $\delta_{\boldsymbol{\alpha}\boldsymbol{\beta}}$ is the multi-index version of the Kronecker delta), and any function which belongs to $\mathbb{L}^2(\rho)$ can be expanded in the basis $(\Psi_{\boldsymbol{\alpha}})_{\boldsymbol{\alpha} \in \mathbb{N}^m}$. Assuming that $\mathcal{M} \in \mathbb{L}^2(\rho)$, the so-called Polynomial Chaos Expansion (PCE) [57] of $\mathcal{M}$ reads:

$$\mathcal{M}(\boldsymbol{\Theta}) = \sum_{\boldsymbol{\alpha} \in \mathbb{N}^m} a_{\boldsymbol{\alpha}} \Psi_{\boldsymbol{\alpha}}(\boldsymbol{\Theta}) \tag{3.6}$$

where $(a_{\boldsymbol{\alpha}})_{\boldsymbol{\alpha}\in\mathbb{N}^m}$ are the PCE coefficients. For each multi-index $\boldsymbol{\alpha}\in\mathbb{N}^m$, the coefficient $a_{\boldsymbol{\alpha}}$ can be interpreted as the coordinate of the orthogonal projection of $\mathcal{M}(\boldsymbol{\Theta})$ on the vector space spanned by $\Psi_{\boldsymbol{\alpha}}$:

$$a_{\boldsymbol{\alpha}} = \langle \mathcal{M}(\boldsymbol{\Theta}) | \Psi_{\boldsymbol{\alpha}} \rangle_\rho = \mathbb{E}\left[\mathcal{M}(\boldsymbol{\Theta})\Psi_{\boldsymbol{\alpha}}(\boldsymbol{\Theta})\right] \tag{3.7}$$

3.1.2. Calculation of PC coefficients

For computational purposes, the PCE representation (3.6) is truncated by using a finite set $\mathcal{A}\subset\mathbb{N}^m$ of multi-indices:

$$\mathcal{M}(\boldsymbol{\Theta}) \approx \widehat{\mathcal{M}}^{PC}(\boldsymbol{\Theta}) = \sum_{\boldsymbol{\alpha}\in\mathcal{A}} a_{\boldsymbol{\alpha}}\Psi_{\boldsymbol{\alpha}}(\boldsymbol{\Theta}) \tag{3.8}$$

Re-indexing the multi-indices $\{\boldsymbol{\alpha}\in\mathcal{A}\}$ by $\{1,\dots,P\}$ with $P=\mathrm{Card}(\mathcal{A})$ yields the following vector notation:

$$\widehat{\mathcal{M}}^{PC} = \boldsymbol{a}^\intercal\boldsymbol{\Psi} \tag{3.9}$$

where $\boldsymbol{a}=(a_1,\dots,a_P)$ and $\boldsymbol{\Psi}=(\Psi_1,\dots,\Psi_P)$. The PCE coefficients $\boldsymbol{a}$ can be computed by using *non-intrusive* methods, from point-wise model evaluations. This refers to projection methods [62, 63], stochastic collocation [64] or regression [65, 66, 67]. In the context of regression approaches, Ordinary Least Squares (OLS) are usually considered [65, 66]. Given an experimental design (ED) $\mathcal{X}=(\boldsymbol{\theta}^{(1)},\dots,\boldsymbol{\theta}^{(K)})$ and the corresponding model outputs $\mathcal{Y}=(\mathcal{M}(\boldsymbol{\theta}^{(1)}),\dots,\mathcal{M}(\boldsymbol{\theta}^{(K)}))$ such approaches aim at solving the following minimization problem:

$$\boldsymbol{a} = \underset{\boldsymbol{a}^*\in\mathbb{R}^P}{\arg\min}\ \|\mathcal{Y}-\mathbf{A}\boldsymbol{a}^*\|^2 \tag{3.10}$$

where $\mathbf{A}$ is the $K\times P$ matrix with coefficients $\mathbf{A}_{ij}=\Psi_j(\boldsymbol{\theta}^{(i)})$, and $\|\cdot\|$ is the Euclidean norm of $\mathbb{R}^P$, *i.e.* $\|\boldsymbol{x}\|^2=\sum_{i=1}^P x_i^2$ for $\boldsymbol{x}=(x_1,\dots,x_P)\in\mathbb{R}^P$. In most cases, PCE representations are *compressible*, in the sense that only few terms are significantly contributing to the variance of the model response. Then, compressive sensing [68] techniques have been recently used in the PCE framework in order to construct sparse PCE with ED of limited sizes. One refers to [69] for an recent in-depth review and benchmark on sparse PCE. Finally, once PCE coefficients are computed, the *generalization error* of the truncated PCE defined by $\mathbb{E}\left[(\mathcal{M}(\boldsymbol{\Theta})-\widehat{\mathcal{M}}(\boldsymbol{\Theta}))^2\right]$ may be estimated by using cross-validation techniques [70]. In this context, the Leave One Out (LOO) error is commonly used as an estimate of the PCE generalization error (see [67] for further details).

3.2. Polynomial Chaos-based Kriging

Polynomial Chaos Kriging (PCK) [42, 43] consists in a Kriging [71] whose trend is given by a PCE:

$$\mathcal{M}(\boldsymbol{\theta}) \approx \widehat{\mathcal{M}}^{PCK}(\boldsymbol{\theta}) = \sum_{\boldsymbol{\alpha}\in\mathcal{A}} a_{\boldsymbol{\alpha}}\Psi_{\boldsymbol{\alpha}}(\boldsymbol{\theta}) + \sigma^2 Z(\boldsymbol{\theta}) \tag{3.11}$$

where $\sum_{\boldsymbol{\alpha}\in\mathcal{A}} a_{\boldsymbol{\alpha}}\Psi_{\boldsymbol{\alpha}}(\boldsymbol{\theta})$ is a truncated PCE, σ^2 the PCK variance and Z a zero-mean stationnary Gaussian process with a correlation kernel $R_Z(\boldsymbol{\theta},\boldsymbol{\theta}';\boldsymbol{\eta})$.

The interest of such formulation is twofold: the trend provides a *global* approximation of the model response on the support $\mathcal{D}_{\boldsymbol{\theta}}$ of input parameters, whereas the Gaussian process enables to catch the *local* variability of the model response. Furthermore, the prediction variance associated to the Gaussian process provides a local error measure for PCK model predictions, which can be used as an indicator of the sparsity of the ED. Indeed, Kriging is an exact interpolating method, in the sense that $\mu_{\widehat{y}}(\boldsymbol{\theta}) = \mathcal{M}(\boldsymbol{\theta})$ and $\sigma_{\widehat{y}}(\boldsymbol{\theta}) = 0,\ \forall\boldsymbol{\theta}\in\mathcal{X}$, where $\mu_{\widehat{y}}(\boldsymbol{\theta})$ and $\sigma_{\widehat{y}}(\boldsymbol{\theta})$ are respectively the Kriging prediction mean and standard deviation at the point $\boldsymbol{\theta}$. Thus, the prediction variance is low near ED points and becomes important in unexplored zones of the parameter space. Such local indicator has been exploited in the framework of adaptive surrogate modeling [39, 43], in order to enrich EDs. Note also that a global error measure consisting in a formulation of LOO error is available for Kriging surrogates [72].

Moreover, it is worth noting that global surrogates such as PCE do not dispose of local error measures as simple and direct as Kriging prediction variance, but rather global error measures, such as the LOO error [67]. The PCK formulation then provides a simple way to assess the local error of PCE predictions. It is also worth noting that recent work of Sudret & Marelli [73] provided a local error estimate for PCE surrogates, based on bootstrap resampling.

The setup of a PCK surrogate model requires the calculation of the PC coefficients $\boldsymbol{a} = (a_{\boldsymbol{\alpha}})_{\boldsymbol{\alpha}\in\mathcal{T}}$ as well as Kriging variance σ^2 and correlation hyper-parameters $\boldsymbol{\eta}$. In this context, Schöbi et al [42] propose two computational approaches, namely Sequential PCK (S-PCK) and Optimal PCK (O-PCK). The first approach consist in constructing a PCE surrogate by using the LAR algorithm [67], and then using this PCE as the trend of a universal Kriging model, whose parameters are calibrated through Maximum Likelihood Estimation (MLE) [74]. The second approach aims at iteratively constructing a PCK by adding polynomials one-by-one to the trend, and selecting the surrogate which minimizes a LOO error estimate. For further details, the reader is referred to [42].

4. Bayesian updating using adaptive PCK within subset simulation

4.1. General framework

The proposed Bayesian updating methodology aims at constructing a PCK surrogate which is enriched in an adaptive way throughout the SuS procedure described by Algorithm 1. Keeping the notations introduced in the previous sections, an initial ED $\mathcal{X}^{(0)} = (\boldsymbol{\theta}^1,\dots,\boldsymbol{\theta}^{K_0})$ of size K_0 is defined. Then, the log-likelihood $L(\boldsymbol{\theta}) = \log\left(\mathcal{L}(\boldsymbol{\theta};\boldsymbol{y})\right)$ in Eq. (2.18) is approximated by a PCK surrogate by using the ED $\mathcal{X}^{(0)}$:

$$L(\boldsymbol{\theta}) \approx \widehat{L}(\boldsymbol{\theta}) = \sum_{\boldsymbol{\alpha}\in\mathcal{T}} a_{\boldsymbol{\alpha}}\Psi_{\boldsymbol{\alpha}}(\boldsymbol{\theta}) + \sigma^2 Z(\boldsymbol{\theta}) \tag{4.1}$$

where the polynomials $(\Psi_{\boldsymbol{\alpha}})_{\boldsymbol{\alpha}\in\mathcal{T}}$ are chosen to be orthonormal with respect to the prior density $\rho(\boldsymbol{\theta})$.

This surrogate model aims at approximating the global behavior of the log-likelihood on the support of the prior distribution. The PCE trend is built by using the LAR-based procedure introduced in [67], in order to provide sparse PCE which can be trained with an ED of small size (typically with $K_0 \sim 10^1 - 10^2$). Substituting the full log-likelihood by its surrogate in the modified LSF expression given by Eq. (2.18) yields a surrogate LSF, given by:

$$\widehat{h}(\boldsymbol{\theta}, p) = \log(p) - \log(c) - \widehat{L}(\boldsymbol{\theta}) \tag{4.2}$$

Firstly, given a prescribed number N of samples per subset, the Monte Carlo Simulation (MCS) step of SuS is performed, by using the surrogate LSF instead of the full one. In this way, samples $\left\{(\boldsymbol{\theta}^{(0,k)}, p^{(0,k)})\right\}_{1\leq k\leq K}$ are generated, and the corresponding log-likelihood values $\left\{\widehat{L}(\boldsymbol{\theta}^{(0,k)})\right\}_{1\leq k\leq K}$ are computed. Then, a critical step is the calculation of an initial value of the BUS normalizing constant c. In the adaptive BUS-SuS approach introduced in [30], this value is set as the largest log-likelihood of the generated samples. In the framework of the proposed approach, a modification of this approach is required: indeed, samples drawn through Monte Carlo sampling which are too far away from the ED $\mathcal{X}^{(0)}$ may lead to inaccurate PCK predictions. This implies to potentially sensibly underestimate the optimal value $c_{opt} = \max \mathcal{L}$, or conversely, to strongly overestimate it and altering the efficiency of the SuS procedure, as mentioned in Section 2.3.3. Consequently, we propose to set the initial value of c as the maximum likelihood on a subset of $\mathcal{S}^{(0)} = \left\{\boldsymbol{\theta}^{(0,k)}\right\}_{1\leq k\leq K}$, formed by points which are not too far away from $\mathcal{X}^{(0)}$. At this point, the question is to define a criterion for filtering points whose predictions are deemed to be not accurate.

A quite natural choice proposed in [37] or [75] is based on the convex hull of the points of the ED. The convex hull of $\mathcal{X}^{(0)}$, denoted by $\mathrm{Conv}(\mathcal{X}^{(0)})$ is the smallest convex set which contains the points of $\mathcal{X}^{(0)}$. If the ED points are sufficiently dense, such set may be seen as the "representativeness domain" of the trained surrogate model. Then, the initial constant c may be set as the maximum surrogate likelihood on this set:

$$c = \max_{\boldsymbol{\theta}\in\mathcal{K}^{(0)}} \exp(\widehat{L}(\boldsymbol{\theta})) \tag{4.3}$$

where $\mathcal{K}^{(0)} = \mathcal{S}^{(0)} \cap \mathrm{Conv}(\mathcal{X}^{(0)})$. The Quickhull algorithm [76] will be used for computing the convex hull, as in [75, 37].

Next, at SuS level $i \geq 1$, the surrogate LSF $\widehat{h_l}$ is used for setting the threshold value h_i (see Algorithm 1). Subsequently, n Markov chain seeds $\left\{(\boldsymbol{\theta}^{(i-1,k)}, p^{(i-1,k)})\right\}_{1\leq k\leq n}$ are selected according to surrogate LSF values. We propose to enrich the ED $\mathcal{X}^{(i-1)}$ of the surrogate log-likelihood $\widehat{L}$, by adding $K_t \geq 1$ new points, based on a point enrichment criterion, which will be described in Section 4.2. A new PCK is then trained on the enriched ED $\mathcal{X}^{(i)}$. The adaptive Conditional Sampling [49] procedure is then launched by using the surrogate LSF, in order to generate the samples $\left\{(\boldsymbol{\theta}^{(i,k)}, p^{(i,k)})\right\}_{1\leq k\leq K}$ of the current subset. Then, the value of the constant c is updated at the end of the SuS stage i. For the same reasons underlined for the MCS step, this constant is the maximum likelihood on the set defined by $\mathcal{K}^{(i)} = \mathrm{Conv}(\mathcal{X}^{(i)}) \cap \left\{\boldsymbol{\theta}^{(i,k)}\right\}_{1\leq k\leq K}$, *i.e.* as $c^* = \max(c, c_i)$, where

$c_i = \max_{\boldsymbol{\theta} \in \mathcal{K}^{(i)}} \exp(\widehat{L}(\boldsymbol{\theta}))$. Such update is *a priori* modifying the definition of the current subset F_i (see Eq. (2.17)) since the latter explicitely depends on the scaling constant. However, as derived in [30], updating the scaling constant c does not affect the distribution of the samples of F_i if its corresponding threshold value h_i is adjusted as follows:

$$h_i^* = h_i + \log \frac{c}{c^*} \tag{4.4}$$

Moreover, we also follow the procedure of [30] aiming at decreasing the dependence of the samples of each subset. Knowing that for a fixed $\boldsymbol{\theta} \in \mathcal{D}_{\boldsymbol{\theta}}$, any $p \in \mathcal{D}_p$ which satisfies $\log(p) \leq \log(c) - L(\boldsymbol{\theta}) + h_i$ lies in the subset F_i, the p component of a sample $(\boldsymbol{\theta}, p) \in F_i$ may be resampled by drawing $p^* \sim \mathcal{U}([0, \min(1, c\exp(h_i)\mathcal{L}(\boldsymbol{\theta})])$. This enables to increase the performance of the BUS procedure, since the rejection of a sample during the MCMC sampling phase implies to duplicate an existing sample.

Then, the SuS procedure is continued until reaching the last subset, *i.e.* until $h_i \leq 0$.

4.2. Point enrichment step

In the framework of active learning structural reliability methods [77, 39, 78], *learning functions* are used in order to measure the information gain related to quantities of interest provided by adding a new point to the ED. In this context, a wide range of functions has been developed, including the *Expected Feasibility Function* (EFF) [77], the so-called *U-function* [39], the *Fraction of Bootstrap Replicates* (FBR) [73] or the *constrained min-max function* [78].

The U-function introduced in [39] is particularly well suited for Kriging-based approaches, by focusing on the accuracy on the sign of the surrogate LSF: sample points with non-positive LSF values are classified as failure points, which traduces in the BUS framework by points which are distributed according to the posterior distribution. Therefore, the potentially important uncertainties on predictions at points which are close to the Limit State Surface (LSS) given by $\partial\mathcal{D}_j = \{(\boldsymbol{\theta}, p) \in \mathcal{D}_{\boldsymbol{\theta}} \times \mathcal{D}_p |\ h_l(\boldsymbol{\theta}, p) = 0\}$ can cause them to change sign, which may lead to misclassification. The U-function aims at selecting points in zones where points are announced to be close to the LSS, and/or where Kriging prediction variance is important [39]. This function is given by:

$$U(\boldsymbol{\theta}, p) = \frac{|\mu_{\widehat{h}}(\boldsymbol{\theta}, p)|}{\sigma_{\widehat{h}}(\boldsymbol{\theta}, p)} \tag{4.5}$$

where $\mu_{\widehat{h}}(\boldsymbol{\theta}, p)$ and $\sigma_{\widehat{h}}(\boldsymbol{\theta}, p)$ are, in turn, the prediction mean and variance of the surrogate LSF given by Eq. (4.2). Note that, for a fixed value of c and $p \in \mathcal{D}_p$, $\widehat{h}(\boldsymbol{\theta}, p)$ is a Gaussian random variable:

$$\widehat{h}(\boldsymbol{\theta}, p) \sim \mathcal{N}\left(\log(p) - \log(c) - \mu_{\widehat{L}}(\boldsymbol{\theta}), \sigma^2_{\widehat{L}}(\boldsymbol{\theta})\right) \tag{4.6}$$

where $\mu_{\widehat{L}}(\boldsymbol{\theta})$ and $\sigma_{\widehat{L}}(\boldsymbol{\theta})$ are the prediction mean and variance of the surrogate log-likelihood (4.1). Therefore,

in the framework of the proposed approach, the U-function (4.5) rewrites:

$$U(\boldsymbol{\theta}, p) = \frac{|\log(p) - \log(c) - \mu_{\widehat{L}}(\boldsymbol{\theta})|}{\sigma_{\widehat{L}}(\boldsymbol{\theta})} \tag{4.7}$$

The *misclassification probability* of a point $(\boldsymbol{\theta}, p) \in \mathcal{D}_{\boldsymbol{\theta}} \times \mathcal{D}_p$ is defined by the probability of having $\mu_{\widehat{h}}(\boldsymbol{\theta}, p) > 0$ and $h(\boldsymbol{\theta}, p) \leq 0$ or *vice-versa*. This probability may be expressed as follows [79, 43]:

$$\mathbb{P}_m(\boldsymbol{\theta}, p) = \Phi\left(-U(\boldsymbol{\theta}, p)\right) = \Phi\left(-\frac{|\log(p) - \log(c) - \mu_{\widehat{L}}(\boldsymbol{\theta})|}{\sigma_{\widehat{L}}(\boldsymbol{\theta})}\right) \tag{4.8}$$

Such probability is bounded between 0 and 0.5. The case $\mathbb{P}_m(\boldsymbol{\theta}, p) \to 0$ corresponds to points whose prediction variance is low, and/or points which are far away from the LSS. Conversely, the case $\mathbb{P}_m(\boldsymbol{\theta}, p) \to 0.5$ corresponds to "dangerous" points, which are close to the LSS and/or whose prediction variance is important.

In the case where only one enrichment point is needed, the latter may be selected as the point which maximizes the misclassification probability (4.8). In the case of multiple point enrichment, clustering techniques [45] applied in the framework of adaptive surrogate modeling for SR analysis [43, 41, 80] enable to efficiently selecting new points. In this paper, the weighted k-means algorithm [45] is considered.

Recall that at SuS stage $i \geq 1$, we dispose of n Markov chain seeds $\left\{(\boldsymbol{\theta}^{(i-1,k)}, p^{(i-1,k)})\right\}_{1 \leq k \leq n}$. As proposed in [43, 41], the weights considered for clustering are set as the corresponding misclassification probabilities $\left\{\mathbb{P}_m(\boldsymbol{\theta}^{(i-1,k)}, p^{(i-1,k)})\right\}_{1 \leq k \leq n}$. However, the surrogate log-likelihood $\widehat{L}(\boldsymbol{\theta})$ is defined on the physical parameter space $\mathcal{D}_{\boldsymbol{\theta}}$, and then does not depend on values of $p \in \mathcal{D}_p$. Hence, performing a clustering in the augmented space $\mathcal{D}_{\boldsymbol{\theta}} \times \mathcal{D}_p$ may lead to redundant enrichment points, since the obtained clusters may lie on a line of the form $\{\boldsymbol{\theta}\} \times \mathcal{D}_p$. Consequently, we propose to perform weighted k-means clustering on the candidate set given by $\left\{\boldsymbol{\theta}^{(i-1,k)}\right\}_{1 \leq k \leq n}$ by using the same misclassification probabilities $\left\{\mathbb{P}_m(\boldsymbol{\theta}^{(i-1,k)}, p^{(i-1,k)})\right\}_{1 \leq k \leq n}$ as weights. This is tantamount to projecting the seeds onto the parameter space $\mathcal{D}_{\boldsymbol{\theta}}$ by using the canonical projection $\mathcal{D}_{\boldsymbol{\theta}} \times \mathcal{D}_p \longrightarrow \mathcal{D}_{\boldsymbol{\theta}}$. In this way, the centroids $\left\{\boldsymbol{\theta}_*^{(j)}\right\}_{1 \leq j \leq K_t}$ of the K_t obtained clusters are selected in order to enrich the ED of the surrogate log-likelihood $\widehat{L}(\boldsymbol{\theta})$. The updated ED of $\widehat{L}(\boldsymbol{\theta})$ is then given by $\mathcal{X}^{(i)} = \mathcal{X}^{(i-1)} \cup \left\{\boldsymbol{\theta}_*^{(j)}\right\}_{1 \leq j \leq K_t}$.

4.3. Stopping criterion

The stopping criterion of the surrogate model learning phase may be defined based on the variability of estimated failure probabilities [74], the stability of the estimated failure domain [43, 78] or learning functions [39, 73]. In this paper, we use the stopping criterion based on the U-function introduced in [39]. At SuS stage i, this criterion writes:

$$\min_{(\boldsymbol{\theta}, p) \in \mathcal{S}_0^{(i)}} U(\boldsymbol{\theta}, p) \geq \epsilon_U \tag{4.9}$$

where $\mathcal{S}_0^{(i)}$ is the set formed by the n Markov chain seeds selected for the i-th subset (see Algorithm 1), and ϵ_U is a threshold value. Following [39], we choose the value $\epsilon_U = 2$, which has provided satisfactory accuracy in several application examples. Choosing this value is tantamount to impose a maximal misclassification probability of $\Phi(-2) \approx 0.023$. Notwithstanding its widespread use, it should be underlined that such value may be too conservative in some cases, for complex LSF functions and/or for high dimensionalities [41]. However, the search for an optimal stopping criterion is out of the scope of this paper, and the reader is referred to [41] for further details about recent improvement strategies.

4.4. Summary of the proposed method

The proposed approach, which will be named BUS-PCK in the following sections, is summarized hereafter:

1. An initial ED $\mathcal{X}^{(0)}$ of size K_0 is selected, in order to build a PCK surrogate $\widehat{L} \approx L$ of the log-likelihood (Eq. (4.1)). This induces the definition of a surrogate LSF $\widehat{h}$ (see Eq. (4.2)).
2. Level 0 of SuS procedure (MCS): K samples are drawn from the prior distribution, and the corresponding surrogate LSF values are computed.
3. Initialize BUS normalizing constant c from the generated sample according to Eq. (4.3). This implies the computation of the convex hull of MCS samples with the Quickhull algorithm [76].
4. At SuS level $i \geq 1$:
   a. The threshold value h_i of the current subset F_i is computed as the $\mathbb{P}_t$-percentile of the surrogate LSF values on the samples of level $i-1$ (with $\mathbb{P}_t = 10\%$, following [29, 30]). The intermediate probability $\mathbb{P}_i = \mathbb{P}(F_i|F_{i-1})$ is then computed (see Algorithm 1).
   b. Learning phase of the PCK surrogate (see Section 4.2): K_t points are added to the ED $\mathcal{X}^{(i-1)}$ at previous SuS level, by using the seeds (*i.e.* the $\mathbb{P}_i K$ samples which are lying in F_i) as candidate points. If the stopping condition of the learning phase is met (see Section 4.3), the PCK surrogate model is deemed to be sufficiently accurate near posterior high-probability zones.
   c. Generation of conditional samples: the population of the next SuS subset is generated by using the aCS MCMC algorithm [49], from the previously identified seeds.
   d. Update the BUS normalizing constant c and the threshold value h_i according to Section 4.1.
   e. Convergence of SuS procedure: if $h_i \leq 0$, the SuS procedure is stopped, and the failure probability $\mathbb{P}_f$ is computed as described in Algorithm 1. The samples of the last SuS level correspond to posterior samples.
5. Set $r = i$ and compute the failure probability $\mathbb{P}_f = \prod_{j=1}^{r}$. Posterior samples are given by the projection on $\mathcal{D}_{\boldsymbol{\theta}}$ of the K samples which lie in the subset $F = F_r$. The model evidence is computed as $\mathcal{Z} = \mathbb{P}_f / c$.

The flowchart of the proposed approach is shown in Fig. 1.

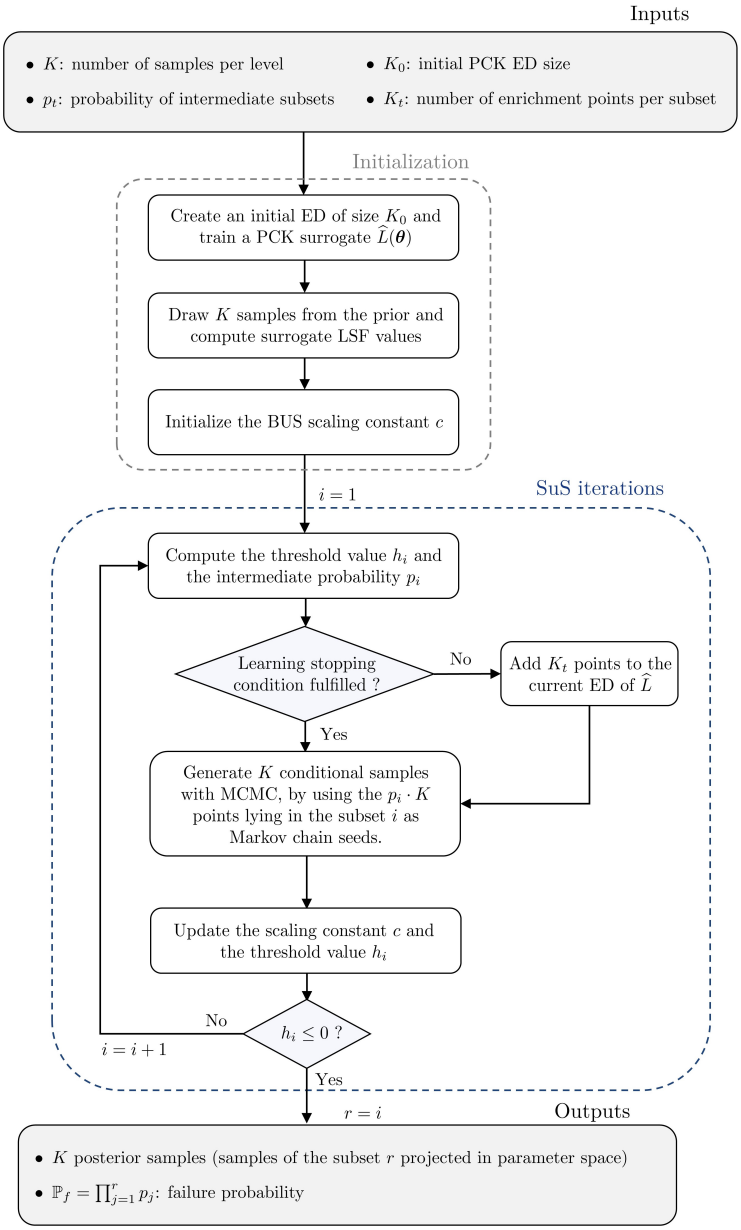

Figure 1: Flowchart of the proposed approach.

5. Case studies

In this section, three case studies of increasing complexity are presented for assessing the performance of the proposed Bayesian updating approach, which will named BUS-PCK in the following. The PCK surrogates will be constructed by using the Optimal PC-Kriging (O-PCK) approach described in [42]. The PCE trends $\sum_{\boldsymbol{\alpha}\in\mathcal{T}} a_{\boldsymbol{\alpha}}\Psi_{\boldsymbol{\alpha}}$ will be constructed by using the classical isotropic truncation sets given by:

$$\mathcal{T}_q = \left\{ \boldsymbol{\alpha} \in \mathbb{N}^m \;\middle|\; \|\boldsymbol{\alpha}\|_1 = \sum_{i=1}^{m} \alpha_i \leq q \right\} \tag{5.1}$$

where $q \leq 10$ is the PCE degree. Sparse PCE are constructed with these truncation sets by using the LAR-based approach introduced in [67]. Moreover, we consider the Matèrn kernel with shape parameter $\nu = \frac{5}{2}$ for all Kriging Gaussian processes. This kernel is given by:

$$R(\|\boldsymbol{\theta} - \boldsymbol{\theta}'\|; \boldsymbol{\eta}) = \prod_{i=1}^{m} \frac{1}{2^{\nu-1}\Gamma(\nu)} \left(\sqrt{2\nu}\frac{|\theta_i - \theta_i'|}{\eta_i}\right)^{\nu} \mathcal{K}_\nu \left(\sqrt{2\nu}\frac{|\theta_i - \theta_i'|}{\eta_i}\right) \tag{5.2}$$

where Γ is the Euler's Gamma function and $\mathcal{K}_\nu$ is the modified Bessel function of the second kind. In this context, we use the software UQLab [81] which provides an implementation of PCK.

The PCK approximation $\widehat{L}(\boldsymbol{\theta})$ of the log-likelihood $L(\boldsymbol{\theta})$ induces the definition of a surrogate posterior PDF:

$$\widehat{\pi}(\boldsymbol{\theta}) = \frac{\rho(\boldsymbol{\theta}) \exp(\widehat{L}(\boldsymbol{\theta}))}{\widehat{\mathcal{Z}}} \tag{5.3}$$

where $\widehat{\mathcal{Z}}$ is the surrogate model evidence:

$$\widehat{\mathcal{Z}} = \int_{\mathcal{D}_{\boldsymbol{\theta}}} \rho(\boldsymbol{\theta}) \exp(\widehat{L}(\boldsymbol{\theta})) \mathrm{d}\boldsymbol{\theta} \tag{5.4}$$

In order to assess the accuracy of the approximation of the posterior PDF, measures taken from information theory are often considered. Indeed, the *Kullback-Leibler Divergence* (KLD) [82] is usually used for measuring the similarity between the surrogate and the true posterior PDF [32], and is defined by:

$$\mathcal{D}_{KL}(\widehat{\pi}||\pi) = \int_{\mathcal{D}_{\boldsymbol{\theta}}} \widehat{\pi}(\boldsymbol{\theta}) \log\left(\frac{\widehat{\pi}(\boldsymbol{\theta})}{\pi(\boldsymbol{\theta})}\right) \mathrm{d}\boldsymbol{\theta} \tag{5.5}$$

This measure does not define a distance in the mathematical sense, especially due to the fact that it is not symmetric, *i.e.* $\mathcal{D}_{KL}(\widehat{\pi}||\pi) \neq \mathcal{D}_{KL}(\pi||\widehat{\pi})$. A symmetrized and somewhat regularized version of KLD is given by the *Jensen-Shannon Divergence* (JSD), defined by [83]:

$$\mathcal{D}_{JS}(\widehat{\pi}||\pi) = \frac{1}{2}\left(\mathcal{D}_{KL}(\widehat{\pi}||\tilde{\pi}) + \mathcal{D}_{KL}(\pi||\tilde{\pi})\right) \tag{5.6}$$

where $\tilde{\pi} = \frac{1}{2}(\widehat{\pi} + \pi)$. In this paper, we will use the *average Jensen-Shannon Divergence* (aJSD) introduced in [23], given by:

$$\overline{\mathcal{D}_{JS}}(\widehat{\pi}||\pi) = \frac{1}{m}\sum_{i=1}^{m} \mathcal{D}_{JS}(\widehat{\pi}_i||\pi_i) \tag{5.7}$$

where $\widehat{\pi}_i$ and π_i are the i-th surrogate and true posterior marginal PDF. This measure enables to summarize the accuracy of the approximation of the posterior PDF in a single scalar, which is computationally affordable since it is based on an average of univariate integrals.

In the following sections, one will consider $K = 5000$ samples per subset, based on [26, 30]. Indeed, in the framework of the numerical examples presented hereafter, such sample size has been observed to be sufficient for exploring the posterior distribution with the SuS procedure [26, 30]. In the general case, when combining the SuS

procedure with surrogate models, it might be possible to consider an "overkill" sample size (*i.e.* $K \sim 10^5 - 10^6$) [84], in order to ensure that all posterior high-probability regions are discovered. The intermediate probability $\mathbb{P}_t$ is chosen as $\mathbb{P}_t = 10\%$, based on [30]. The SuS procedure described in Section 2.3 is first applied by using the full model, and the corresponding results will be considered as a reference. Regarding to the proposed approach, varying initial ED sizes K_0 and ratios $\kappa = K_t/K_0$ will be considered. Moreover, 50 replications of the calculations will be produced.

5.1. One-dimensional analytical function

5.1.1. Problem description

The first case study focuses on a one-dimensional analytical function, which presents a combination of a global trend and a localized behavior:

$$\mathcal{M}(\theta) = 1 + \cos\left(\frac{\theta}{2}\right) + 3\exp(-4(\theta - 2)^2) \tag{5.8}$$

The first two terms may be well approximated by a low-order PCE, whereas the third term induces a peak which requires a sensibly high PCE degree for providing an accurate approximation. Hence, such behavior would make classical PCE-based Bayesian inversions fail, since global approximations are not sufficient here to accurately mimic the model near the high-likelihood zone (around $\theta = 2$). One considers a random variable Θ with prior $\mathcal{N}(0, 1)$, an observation data $y = \mathcal{M}(2) = 4.54$ and an additive Gaussian discrepancy model with noise variance $\sigma = 0.4$. This leads to the following likelihood function:

$$\mathcal{L}(\theta; y) = \frac{1}{\sqrt{2\pi}\sigma} \exp\left(-\frac{1}{2\sigma^2}(\mathcal{M}(\theta) - y)^2\right) \tag{5.9}$$

5.1.2. Posterior distribution

First, the proposed methodology is illustrated in Fig.2, for the case $K_0 = 20$ and $\kappa = 0.2$. At level 0 of SuS procedure, a PCK surrogate model of the log-likelihood is built on the initial ED $\mathcal{X}^{(0)}$ of size K_0. The points of $\mathcal{X}^{(0)}$ are sensibly dense around the prior mean $\theta = 0$, whereas the log-likelihood peak is located near $\theta \approx 2$. As shown in Fig.2a, the predictions of the PCK surrogate for $\theta \geq 2$ are sensibly uncertain and overestimate the log-likelihood, which leads to indicate a wrong location of the posterior high-probability zone. Then, at SuS level 1, the point enrichment step described in Section 4.2 enables to select $K_t = \kappa K_0$ new points $\mathcal{X}_{new} = \left\{\boldsymbol{\theta}_*^{(i)}\right\}_{1 \leq i \leq 4}$ to add to the ED, based on the misclassification probability given in Eq.(4.8). These points locate in the vicinity of the log-likelihood peak, near $\theta \approx 2$, as shown by the white diamonds in Fig. 2. Then, the PCK surrogate model is updated, by using the ED $\mathcal{X}^{(1)} = \mathcal{X}^{(0)} \cup \mathcal{X}_{new}$. The predictions of the updated surrogate model are sensibly more accurate near the log-likelihood peak, as underlined by Fig.2b.

Then, the convergence of JSD with respect to the effective number of model calls denoted by $\mathbb{E}[N_c]$ is shown in Fig.3. For a single run, the number of model calls is given by $N_c = K_0(1 + n_S\kappa)$, where n_S is the number

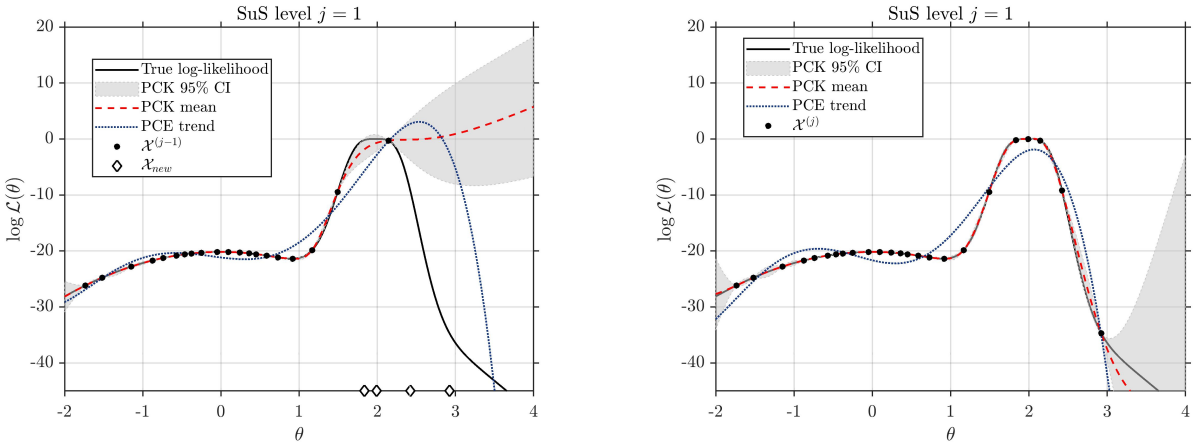

(a) Before point enrichment

(b) After point enrichment

Figure 2: 1D analytical function: illustration of the proposed method at SuS level 1

of subsets required for stopping the SuS procedure. For moderate ED sizes $K_0 \approx 50$, the proposed approach is more efficient than its non-adaptive counterpart ($\kappa = 0$), since the JSD for $\kappa \geq 0.1$ is at least one order of magnitude smaller than that for $\kappa = 0$. In the case of larger EDs, JSD values for $\kappa \in \{0, 0.1, 0.2\}$ are closer, which can be explained by the fact that more informative points (*i.e.* with high likelihood) are drawn during the initial sampling step aiming at constructing the initial ED of the surrogate model. For a fixed amount of model calls, the JSD decreases when κ increases, though. This underlines the efficiency of the point enrichment step, which enables to better focus on high-likelihood zones for enriching the surrogate model.

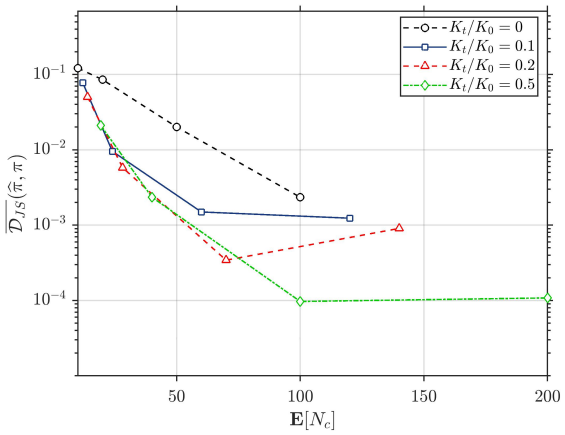

Figure 3: 1D analytical function: convergence of JSD with respect to the average number of model calls $\mathbb{E}[N_c]$.

The posterior PDF obtained with the reference calculations and the proposed approach are shown in Fig. 4. Visual inspection of PDF confirms the analysis of the convergence of JSD, since the reference posterior PDF is well approximated by its surrogate counterpart as the experimental size increases. Lastly, several QoI obtained from calculations, namely the effective number of model calls $\mathbb{E}[N_c]$, the posterior mean $\mathbb{E}[\theta|y]$, the standard deviation $\sqrt{\mathbf{Var}[\theta|y]}$, and the model evidence $\mathcal{Z}$ are summarized in Tab. 1. The corresponding relative errors $\epsilon = |\chi - \chi_{ref}|/\chi_{ref}$ are given in brackets, in %. The results emphasize the efficiency of the BUS-PCK approach, since a satisfactory approximation of the posterior PDF is provided for $\mathbb{E}[N_c] = 100$ model calls, which represents

a reduction of 99.3% of the full cost of the SuS procedure described in Section 2.3, namely $1.5 \cdot 10^4$ full model calls.

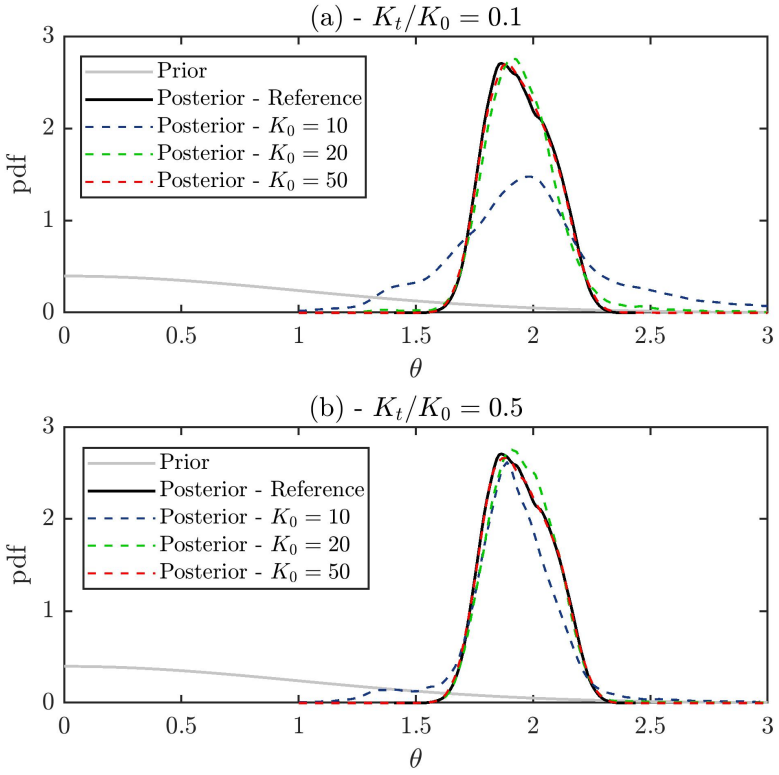

Figure 4: 1D analytical function: prior and posterior PDF: (a) $K_t/K_0 = 0.1$; (b) $K_t/K_0 = 0.5$.

	K_0	K_t/K_0	$\mathbb{E}[N_c]$	$\mathbb{E}[\theta\|y]$	$\sqrt{\mathbf{Var}[\theta\|y]}$	$\mathcal{Z}$
BUS-PCK	20	0.1	24	1.938 (0.2)	0.213 (59.3)	0.028 (16.1)
	20	0.5	40	1.954 (0.6)	0.147 (10.1)	0.037 (53.3)
	50	0.1	60	1.944 (0.1)	0.168 (25.4)	0.025 (4.2)
	50	0.5	100	1.942 (0.0)	0.138 (3.4)	0.025 (3.4)
	100	0.1	120	1.941 (0.0)	0.148 (10.5)	0.024 (0.1)
	100	0.5	200	1.942 (0.0)	0.134 (0.4)	0.024 (0.6)
Reference			**15000**	**1.942**	**0.134**	**0.024**

Table 1: 1D analytical function: posterior QoI, with relative errors in %.

5.2. Two degrees-of-freedom shear building

5.2.1. Problem description

The second case study was originally introduced in [85], and then studied in [30, 37, 25, 38], and involves a two degrees-of-freedom shear building, shown in Fig. 5. The problem consists in estimating the posterior inter-story stiffnesses of the structure, based on measurements of the eigen-frequencies of the structure.

The inter-story stiffnesses are set as $k_i = \Theta_i k_n$ for $i \in \{1, 2\}$, where $k_n = 29.7 \cdot 10^6$ N.m^{-1} and Θ_1, Θ_2

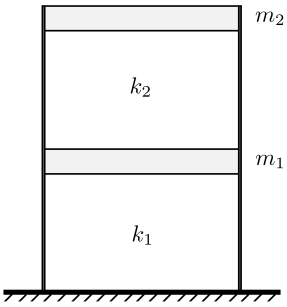

Figure 5: Two degrees-of-freedom shear building

are random variables endowed with lognormal priors with modes 1.3 and 0.8, and standard deviations equal to 1. The masses of the two stories are supposed to be deterministic, and are set as $m_1 = 16.531 \cdot 10^3$ kg and $m_2 = 16.131 \cdot 10^3$ kg. Two measured eigen-frequencies $\tilde{\boldsymbol{f}} = (\tilde{f}_1, \tilde{f}_2)$ will be used for Bayesian updating, with $\tilde{f}_1 = 3.13$ Hz and $\tilde{f}_2 = 9.83$ Hz. The corresponding likelihood function writes:

$$\mathcal{L}(\boldsymbol{\theta}; \tilde{\boldsymbol{f}}) = \exp\left(-\frac{J(\boldsymbol{\theta})}{2\sigma^2}\right) \tag{5.10}$$

where $\sigma = 1/16$ and $J(\boldsymbol{\theta})$ is the modal measure-of-fit function given by [85]:

$$J(\boldsymbol{\theta}) = \sum_{i=1}^{2} \mu_i^2 \left(\frac{f_i(\boldsymbol{\theta})^2}{\tilde{f}_i^2} - 1\right)^2 \tag{5.11}$$

with $\mu_1 = \mu_2 = 1$, and $(f_i(\boldsymbol{\theta}))_{i\in\{1,2\}}$ are the eigen-frequencies obtained by solving the equation of motion for un-damped free vibration applied to the structure. This equation is given by:

$$\mathbf{M}\ddot{\boldsymbol{u}} + \mathbf{K}\boldsymbol{u} = \mathbf{0} \tag{5.12}$$

where $\mathbf{M} = \begin{pmatrix} m_1 & 0 \\ 0 & m_2 \end{pmatrix}$ is the mass matrix and $\mathbf{K} = \begin{pmatrix} k_1 + k_2 & -k_2 \\ -k_2 & k_2 \end{pmatrix}$ is the stiffness matrix, and $\boldsymbol{u} = (u_1, u_2)^\intercal$ the displacement vector.

The posterior distribution of the parameters $\boldsymbol{\Theta} = (\Theta_1, \Theta_2)$ is bi-modal with significantly distant modes [85, 37], which makes the problem difficult to solve when using classical MCMC sampling approaches.

5.2.2. Posterior distribution

The proposed approach is applied by considering $K_0 \in \{20, 50, 100, 200\}$ and $\kappa \in \{0, 0.1, 0.2, 0.5\}$.

Fig. 6 illustrates the proposed approach in the framework of the previously presented mechanical problem, with $K_0 = 50$ and $K_t = 10$. Firstly, an initial ED formed by samples drawn from the prior is defined, and the surrogate log-likelihood is subsequently trained. The first step of SuS procedure enables to identify $\mathbb{P}_t K = 500$ seeds, to generate the population of the first subset. As shown in Fig. 6a, most of these seeds lie outside

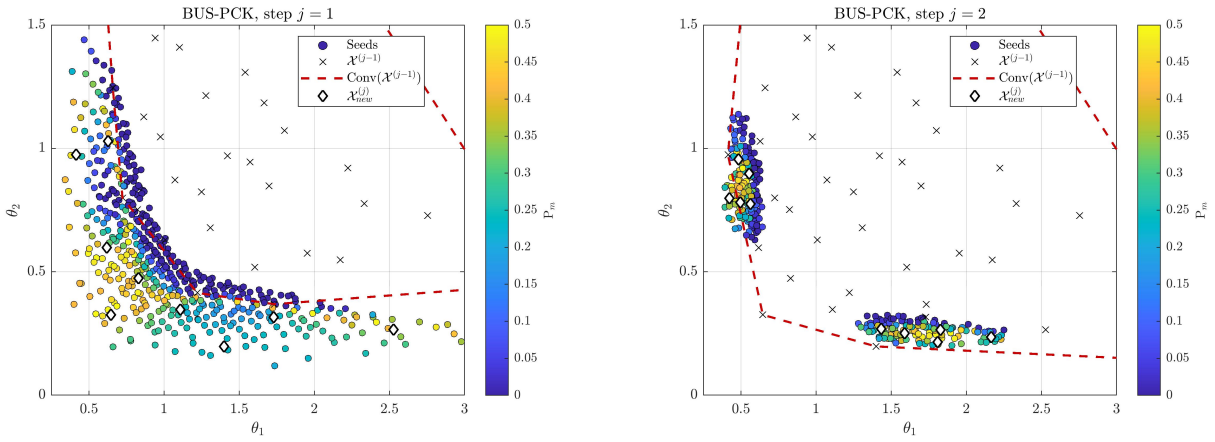

(a) SuS level 1

(b) SuS level 2

Figure 6: Two DOF structure: misclassification probability of seeds and enrichment of the ED of the surrogate log-likelihood at SuS levels 1 & 2.

the convex hull of the current ED. Moreover, the misclassification probability (see Eq. 4.8) of such seeds is sensibly important, which indicates that log-likelihood predictions are classifying posterior points outside of the ED convex hull, and/or predictions are significantly uncertain in such zones. The weighted k-means clustering proposed in Section 4.2 enables to select enrichment points (white diamonds in Fig. 6a) which are quite uniformly spaced outside from the convex hull of the current ED. The surrogate model is then updated, by using the new ED. As shown in Fig.6b, the ED convex hull has been enlarged, and the seeds of SuS level 2 are mostly lying in it, and form two clusters. Then, the point enrichment step proposes K_t new candidate points which are located in these clusters. In this way, the accuracy of predictions provided by the surrogate model is improved specifically in these zones, which correspond to the posterior support.

Next, the convergence of aJSD (5.7) with respect to $\mathbb{E}[N_c]$ is shown in Fig. 7. The proposed methodology is significantly more efficient when $\kappa > 0$, since aJSD values for $\kappa > 0$ are about two orders of magnitude smaller than those for $\kappa = 0$, for a given ED size (see Fig. 7b). In the non-adaptive case ($\kappa = 0$), the aJSD is converging much more slower as the ED size increases. This is due to the fact that the posterior support is located in low-probability zones of the prior (see Fig. 6). Then, without adaptive point enrichment, a very large ED size K_0 is required to draw a sufficient amount of informative points. In this context, the proposed point enrichment method based on clustering is well suited to the problem, since it allows to enrich the surrogate log-likelihood near the posterior high-probability zones, even in the case of a non-connected posterior support.

Then, the contours of the posterior joint PDF obtained with reference calculations and the proposed approach for $K_0 = 200$ and $\kappa = 0.2$ are shown in Fig. 8. The shape of the joint posterior is well approximated by the proposed approach, with a limited amount of model calls ($\sim 10^2$). Furthermore, the location of posterior modes is well reproduced. QoI related to left and right clusters of the identified posterior are summarized in Tab. 2 & 3. An average number of model calls of $\mathbb{E}[N_c] = 320$ is sufficient to provide an accurate approximation of the posterior PDF, which represents a reduction of about 98.4% of the total cost of $2 \cdot 10^4$ model calls required by using the full likelihood function.

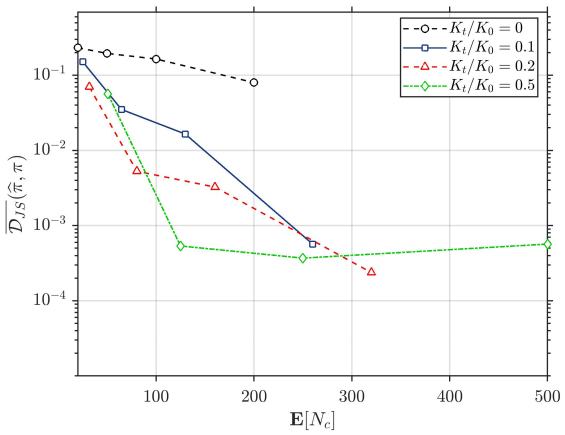

Figure 7: 2 DOF structure: convergence of aJSD with respect to $\mathbb{E}[N_c]$.

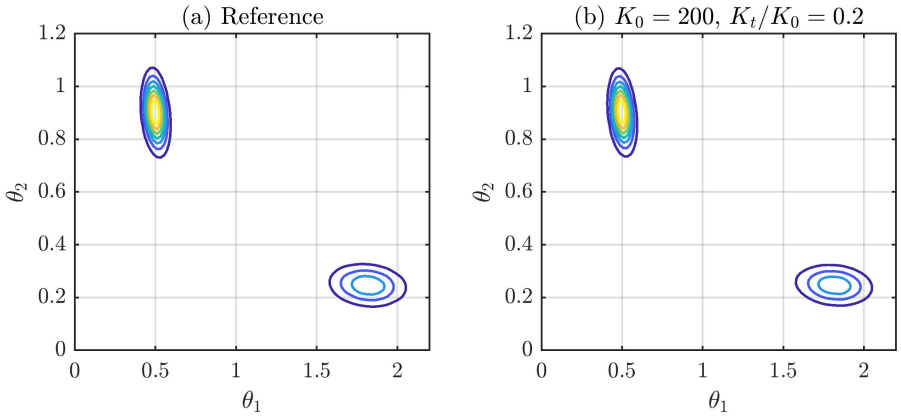

Figure 8: Contours of the posterior joint PDF: (a) Reference; (b) $K_0 = 200$ and $K_t/K_0 = 0.2$.

	K_0	K_t/K_0	$\mathbb{E}[N_c]$	$\mathbb{E}[\theta_1\|\tilde{\boldsymbol{f}}]$	$\mathbb{E}[\theta_2\|\tilde{\boldsymbol{f}}]$	$\sqrt{\mathbf{Var}[\theta_1\|\tilde{\boldsymbol{f}}]}$	$\sqrt{\mathbf{Var}[\theta_2\|\tilde{\boldsymbol{f}}]}$	$\mathcal{Z}$ $(\times 10^{-3})$
BUS-PCK	50	0.2	80.4	0.502 (0.0)	0.893 (0.7)	0.044 (18.8)	0.086 (23.9)	1.484 (1.3)
	50	0.5	125	0.502 (0.0)	0.898 (0.1)	0.039 (3.5)	0.073 (3.9)	1.474 (1.9)
	100	0.2	160	0.505 (0.6)	0.887 (1.4)	0.045 (21.3)	0.085 (22.0)	1.618 (7.6)
	100	0.5	250	0.502 (0.0)	0.899 (0.0)	0.039 (3.0)	0.072 (2.9)	1.485 (1.2)
	200	0.2	320	0.501 (0.2)	0.900 (0.1)	0.038 (2.1)	0.070 (0.9)	1.509 (0.4)
	200	0.5	500	0.502 (0.0)	0.899 (0.0)	0.038 (0.6)	0.070 (0.3)	1.483 (1.3)
Reference			**20000**	**0.502**	**0.899**	**0.037**	**0.070**	**1.503**

Table 2: 2 DOF structure: posterior QoI related to the left cluster, with relative errors in %.

5.3. Multimodal mixture of Gaussians

5.3.1. Problem description

The third case study is introduced in [86], and involves a mixture of Gaussian distributions. A uniform prior

	K_0	K_t/K_0	$\mathbb{E}[N_c]$	$\mathbb{E}[\theta_1\|\tilde{\boldsymbol{f}}]$	$\mathbb{E}[\theta_2\|\tilde{\boldsymbol{f}}]$	$\sqrt{\mathbf{Var}[\theta_1\|\tilde{\boldsymbol{f}}]}$	$\sqrt{\mathbf{Var}[\theta_2\|\tilde{\boldsymbol{f}}]}$	$\mathcal{Z}$ $(\times 10^{-3})$
BUS-PCK	50	0.2	80.4	1.811 (0.2)	0.245 (0.8)	0.178 (25.7)	0.022 (17.9)	1.484 (1.3)
	50	0.5	125	1.812 (0.1)	0.246 (0.2)	0.144 (1.8)	0.020 (5.9)	1.474 (1.9)
	100	0.2	160	1.801 (0.7)	0.246 (0.3)	0.154 (8.5)	0.021 (11.9)	1.618 (7.6)
	100	0.5	250	1.813 (0.1)	0.246 (0.2)	0.144 (1.3)	0.019 (3.6)	1.485 (1.2)
	200	0.2	320	1.814 (0.0)	0.247 (0.0)	0.143 (0.9)	0.019 (0.5)	1.509 (0.4)
	200	0.5	500	1.814 (0.0)	0.247 (0.0)	0.144 (1.3)	0.019 (2.1)	1.483 (1.3)
Reference			**20000**	**1.814**	**0.247**	**0.142**	**0.019**	**1.503**

Table 3: 2 DOF structure: posterior QoI related to the right cluster, with relative errors in %.

over the square $[0, a] \times [0, a]$ is considered, whereas the likelihood function is defined by:

$$\mathcal{L}(\boldsymbol{\theta}; \{\boldsymbol{\mu}_j\}) = \sum_{j=1}^{n} w_j \varphi_2(\boldsymbol{\theta}; \boldsymbol{\mu}_j, \sigma) \tag{5.13}$$

where the $\{\boldsymbol{\mu}_j\}$ are drawn from the prior $\mathcal{U}([0, a] \times [0, a])$, $\{w_j\}$ are the weights of the mixture, and $\varphi_2(\cdot; \boldsymbol{\mu}_j, \sigma)$ is the PDF of the bivariate Gaussian distribution $\mathcal{N}(\boldsymbol{\mu}_j, \sigma^2 \mathbf{I})$. We set $a = 10$, $\sigma = 0.1$, $n = 10$ and $w_j = 1/n$ for all $j \in \{1, \ldots, n\}$. The corresponding posterior PDF $\pi(\boldsymbol{\theta}; \{\boldsymbol{\mu}_j\}) \propto \mathbf{1}_{[0,a]^2}(\boldsymbol{\theta}) \mathcal{L}(\boldsymbol{\theta}; \{\boldsymbol{\mu}_j\})$ is multimodal, with 10 modes. This is illustrated in Fig. 9, where contours of the likelihood function are presented.

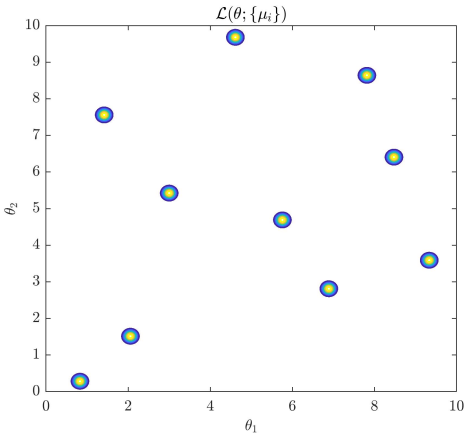

Figure 9: Multimodal Gaussian mixture: contours of likelihood function

5.3.2. Posterior distribution

The proposed approach is applied by considering $K_0 \in \{50, 100, 150, 250\}$ and $\kappa \in \{0, 0.1, 0.2\}$. Fig. 10 presents a comparison between posterior samples drawn with the SuS procedure (see Section 2.3) and samples drawn with the proposed approach, for $K_0 \in \{100, 150, 250\}$ and $\kappa = 0.2$. Firstly, as depicted by Fig. 10a, the posterior samples obtained with the aBUS-SuS algorithm separate into 10 significantly spaced clusters. This underlines the complexity of the posterior PDF, which would be difficult to sample by using classical MCMC

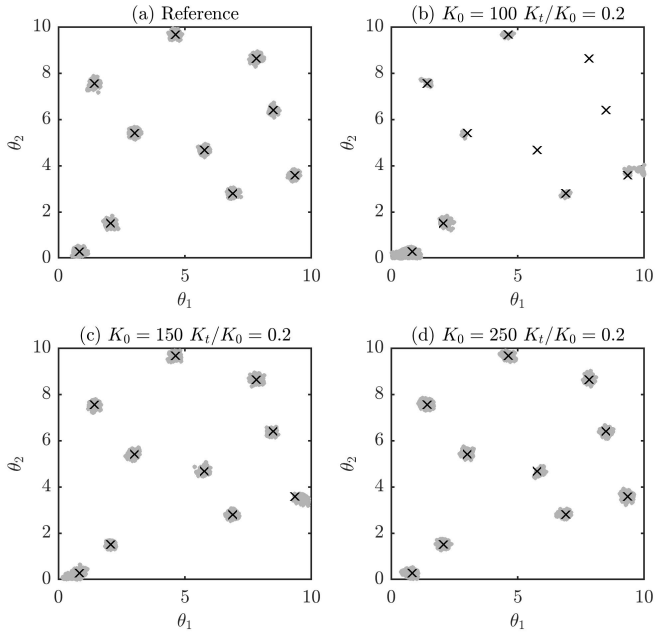

Figure 10: Multimodal Gaussian mixture: reference (a) and BUS-PCK-based (b-d) posterior samples (sample size: $5 \cdot 10^3$). *Black crosses ($\times$) represent the modes $\{\boldsymbol{\mu}_j\}$ of the posterior distribution.*

approaches, for which the generated Markov chains may be trapped near few modes [86].

Next, for $K_0 = 100$ and $\kappa = 0.2$, the proposed approach completely misses 3 modes (see Fig. 10b). When $K_0 = 150$ and $\kappa = 0.2$, the proposed approach correctly identifies the 10 modes of the posterior (see Fig. 10c), even though the spread of the clusters near $(0, 0)$ and $(10, 3)$ is roughly approximated. Lastly, the 10 modes of the posterior are well reproduced when $K_0 = 250$ and $\kappa = 0.2$ (see Fig. 10d).

The convergence of aJSD (5.7) with respect to $\mathbb{E}[N_c]$ is shown in Fig. 11. First, when no surrogate model adaptation is performed (*i.e.* $\kappa = 0$), the aJSD stagnates around a value of 10^{-1}. This may be explained by the highly localized behavior of the likelihood function, which seems to be difficult to approximate with a fixed ED built from the uniform prior $\mathcal{U}([0, a] \times [0, a])$. For a given number of full likelihood calls, significantly lower aJSD values are obtained when $\kappa > 0$. In particular, when $\mathbb{E}[N_c] \geq 200$, the aJSD with $\kappa = 0.2$ is approximately two orders of magnitude smaller than aJSD in the case $\kappa = 0$. This underlines the efficiency of the proposed adaptive point enrichment scheme, as mentioned in the example presented in Section 5.2. The proposed approach takes advantage of the local features provided by the Gaussian process of the PCK surrogate for better catching the likelihood behavior near the modes $\{\boldsymbol{\mu}_j\}$ of the posterior.

Finally, QoI related to the posterior distribution are summarized in Tab. 4. For the sake of brevity, only the components of the posterior mean $\mathbb{E}\left[\boldsymbol{\theta}|\{\boldsymbol{\mu}_j\}\right]$ and the standard deviation $\sqrt{\mathbf{Var}\left[\boldsymbol{\theta}|\{\boldsymbol{\mu}_j\}\right]}$ are considered as QoI, rather than considering the statistics of each of the 10 clusters of the posterior. The proposed approach provides correct estimates of $\mathbb{E}\left[\theta_i|\{\boldsymbol{\mu}_j\}\right]$ and $\sqrt{\mathbf{Var}\left[\theta_i|\{\boldsymbol{\mu}_j\}\right]}$ from $K_0 = 100$ and $\kappa = 0.2$. Moreover, fair estimates of the model evidence $\mathcal{Z}$ are obtained with $K_0 = 150$ and $\kappa = 0.2$. Finally, it is worth noting that the proposed

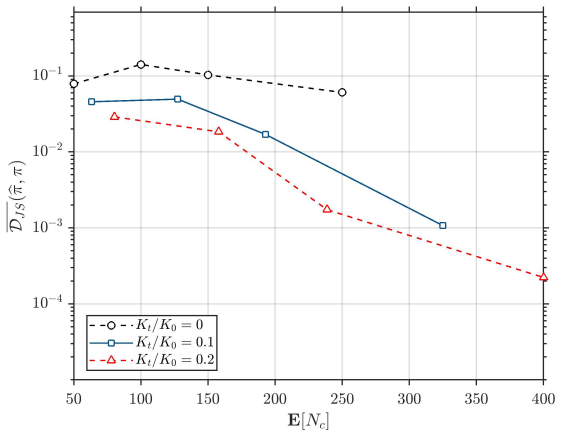

Figure 11: Multimodal Gaussian mixture: convergence of aJSD with respect to $\mathbb{E}[N_c]$

method provides a quite good approximation of the posterior with a number of full likelihood evaluations of about $\mathbb{E}[N_c] \approx 240$ (see Tab. 4), which corresponds to a reduction of about 98.8% of the total cost of $2 \cdot 10^4$ full likelihood evaluations required by a direct application of the SuS procedure.

	K_0	K_t/K_0	$\mathbb{E}[N_c]$	$\mathbb{E}[\theta_1 \vert \{\boldsymbol{\mu_j}\}]$	$\mathbb{E}[\theta_2 \vert \{\boldsymbol{\mu_j}\}]$	$\sqrt{\mathbf{Var}[\theta_1 \vert \{\boldsymbol{\mu_j}\}]}$	$\sqrt{\mathbf{Var}[\theta_2 \vert \{\boldsymbol{\mu_j}\}]}$	$\mathcal{Z}$
BUS-PCK	100	0.1	127.4	4.323 (14.6)	4.309 (13.8)	2.730 (7.2)	2.960 (2.2)	0.063 (525.4)
	100	0.2	158	4.584 (9.5)	4.778 (4.4)	2.825 (3.9)	2.986 (3.1)	0.046 (352.0)
	150	0.1	192.9	4.590 (9.4)	4.794 (4.1)	2.857 (2.9)	2.949 (1.8)	0.024 (138.0)
	150	0.2	238.8	5.069 (0.1)	4.921 (1.5)	2.954 (0.4)	2.852 (1.5)	0.012 (16.3)
	250	0.1	325	5.053 (0.2)	4.830 (3.4)	2.901 (1.4)	2.843 (1.8)	0.011 (4.4)
	250	0.2	400	5.058 (0.1)	4.953 (0.9)	2.927 (0.5)	2.885 (0.4)	0.010 (2.7)
Reference			**20000**	**5.065**	**4.998**	**2.941**	**2.896**	**0.010**

Table 4: Multimodal Gaussian mixture: posterior QoI, with relative errors in %.

5.4. Diffusion problem

5.4.1. Problem description

The last case study consists in a 1D diffusion problem introduced in [26], as the steady state version of the problem studied in [33]. The problem is described by the following diffusion equation on the domain $\mathcal{D} = [0, 1]$:

$$\nabla \left(a(x) \nabla u(x) \right) + b(x) = 0 \tag{5.14}$$

where the diffusivity $a(x)$ is represented by a random field, and the source term $b(x)$ is given by:

$$b(x) = \sum_{i=1}^{N} \frac{s_i}{\sqrt{2\pi}\sigma_i} \exp\left(-\frac{(l_i - x)^2}{2\sigma_i^2} \right) \tag{5.15}$$

This term corresponds to N localized sources with locations $(l_i)_{1 \leq i \leq N}$ and strengths $(s_i)_{1 \leq i \leq N}$ and widths $(\sigma_i)_{1 \leq i \leq N}$. One considers $N = 3$ sources at locations $l_1 = 0.25$, $l_2 = 0.5$ and $l_3 = 0.75$. The strengths

are assumed to be identical, and are set as $s_i = 10$, as well as the widths, which are fixed to $\sigma_i^2 = 10^{-3}$. Furthermore, Dirichlet boundary conditions $u(0) = u(1) = 0$ are adopted for solving Eq. (5.14). The diffusion equation (5.14) is solved by using linear finite elements, on a uniform grid with spacing $\Delta x = \frac{1}{48}$.

The problem consists in inferring the diffusivity $a(x)$ from noisy measurements of the field $u(x)$, provided by a set of $n = 11$ sensors uniformly spaced in $\mathcal{D}$ (excluding the endpoints). The prior of the log-diffusivity $\log a$ is supposed to be a Gaussian stationnary random field, with mean $\mu_{\log a} = 0.1$ and standard deviation $\sigma_{\log a} = 0.2$, and an exponential correlation kernel:

$$R_{\log a}(x, x') = \exp\left(-\frac{|x - x'|}{\ell_c}\right) \tag{5.16}$$

with $\ell_c = 0.3$.

The log-diffusivity random field is represented by a truncated Karhunen-Loève (KL) [87, 57] expansion:

$$\log a(x) \approx \mu_{\log a} + \sum_{i=1}^{m} \sqrt{\lambda_i}\zeta_i\phi_i(x) \tag{5.17}$$

where $m = 10$ [26], $(\zeta_i)_{1\leq i\leq m}$ are the m first KL eigenmodes, and $(\lambda_i, \phi_i)_{1\leq i\leq m}$ are the eigenvalues and eigenfunctions associated to the covariance kernel $\Sigma_{\log a}(x, x') = \sigma^2_{\log a} R_{\log a}(x, x')$. The latter are satisfying the Fredholm integral equations of the second kind:

$$\int_{\mathcal{D}} \Sigma_{\log a}(x, x')\phi_i(x')\mathrm{d}x' = \lambda_i\phi_i(x) \tag{5.18}$$

which can be solved analytically in the case of exponential kernels [57].

Then, synthetic data is generated from a realization of the log-diffusivity random field, by computing the corresponding field $u(x)$ at sensors locations and adding to it a Gaussian noise term with zero mean and standard deviation $\sigma_u = 0.1$. In order to avoid to commit an *inverse crime* [1], this synthetic data is generated by using a much finer grid for solving Eq. (5.14). The $m = 10$ first KL eigenmodes $(\zeta_i)_{1\leq i\leq m}$ are subsequently inferred from the generated data.

5.4.2. Posterior distribution

The proposed approach is applied by considering $K_0 \in \{50, 100, 250, 500\}$ and $\kappa \in \{0, 0.1, 0.2\}$. The convergence of aJSD (5.7) with respect to $\mathbb{E}[N_c]$ is shown in Fig. 12. The performance of the approach depends less on the adaptation step of the surrogate model, since the aJSD presents a similar behavior for $\kappa = 0$ and $\kappa > 0$. However, for moderate to large ED sizes ($\approx 250 - 500$), the adaptive point enrichment provides a slightly smaller aJSD than in the non-adaptive case ($5 \cdot 10^{-3}$ when $\kappa = 0$ and 10^{-3} when $\kappa > 0$). Such behavior may be explained by the fact that most of the posterior mass is enclosed in high-probability zones of the prior. In this case, the adaptive point enrichment targets zones in which samples are frequently drawn when sampling from the prior.

This clearly underlines the difference of performance between the present diffusion problem and the mechanical problem presented in Section 5.2, which presented a bi-modal with support located in low-probability zones of the prior.

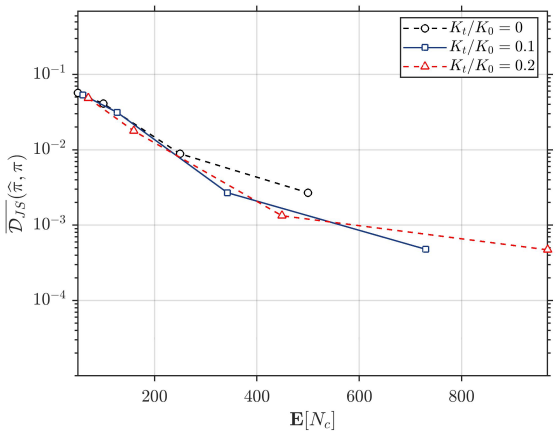

Figure 12: Diffusion problem: convergence of aJSD with respect to $\mathbb{E}[N_c]$.

Then, it is worth noting that the *active dimensionality* of the problem is limited to 6, since the posterior distribution of the four last KL eigenmodes is sensibly close to their prior distribution. This has been often encountered in the framework of UQ benchmark problems related to diffusion with random diffusivity fields [23]. Consequently, the following analysis will be then focused on the six first KL eigenmodes.

The posterior univariate and bivariate PDF of the six first KL eigenmodes are shown in Fig.13. The reference PDF and those obtained for $K_0 = 250$ and $\kappa = 0.1$ are compared. The shape of the posterior distribution is well approximated with the proposed approach, with a quite limited amount of model calls (≈ 350). In particular, the correlation structure is well reproduced, notably regarding to the couples (ζ_1, ζ_3) and (ζ_2, ζ_4) which exhibit quite strong linear correlations. Posterior mean and standard deviation values are summarized in Tab. 5 & 6. It is also worthwhile noting that the following approach provides a fair estimate of the model evidence with a quite moderate amount of model calls ($\approx 350 - 500$), as underlined by Tab. 7 which summarizes values of the model evidence. As mentioned earlier, a quite important advantage of the proposed approach is that it enables to compute the model evidence as a by-product of the SuS procedure (see Algorithm 1). Classical MCMC approaches do not enable to estimate the model evidence once the sampling procedure is performed.

$\mathbb{E}[\zeta_i \vert \boldsymbol{d}]$	K_0	K_t/K_0	$\mathbb{E}[N_c]$	ζ_1	ζ_2	ζ_3	ζ_4	ζ_5	ζ_6
BUS-PCK	100	0.1	127	-0.55 (23.4)	-0.13 (68.1)	0.71 (29.6)	-0.57 (41.2)	0.05 (116.0)	-0.54 (46.0)
	100	0.2	159.6	-0.59 (17.2)	-0.26 (33.0)	0.76 (24.4)	-0.72 (24.7)	-0.01 (95.9)	-0.80 (20.1)
	250	0.1	342.5	-0.70 (2.9)	-0.41 (3.0)	0.96 (4.3)	-0.89 (7.8)	-0.22 (27.0)	-0.96 (5.1)
	250	0.2	449	-0.70 (2.6)	-0.40 (2.3)	0.97 (3.8)	-0.93 (3.6)	-0.23 (22.1)	-0.96 (5.2)
	500	0.1	730	-0.71 (1.1)	-0.37 (6.5)	0.99 (1.7)	-0.91 (5.2)	-0.28 (5.0)	-1.02 (1.2)
	500	0.2	968	-0.72 (0.1)	-0.38 (4.8)	1.01 (0.3)	-0.92 (4.3)	-0.30 (2.8)	-1.03 (2.6)
Reference			**27600**	**-0.72**	**-0.39**	**1.00**	**-0.96**	**-0.30**	**-1.01**

Table 5: Diffusion problem: posterior means of few KL eigenmodes.

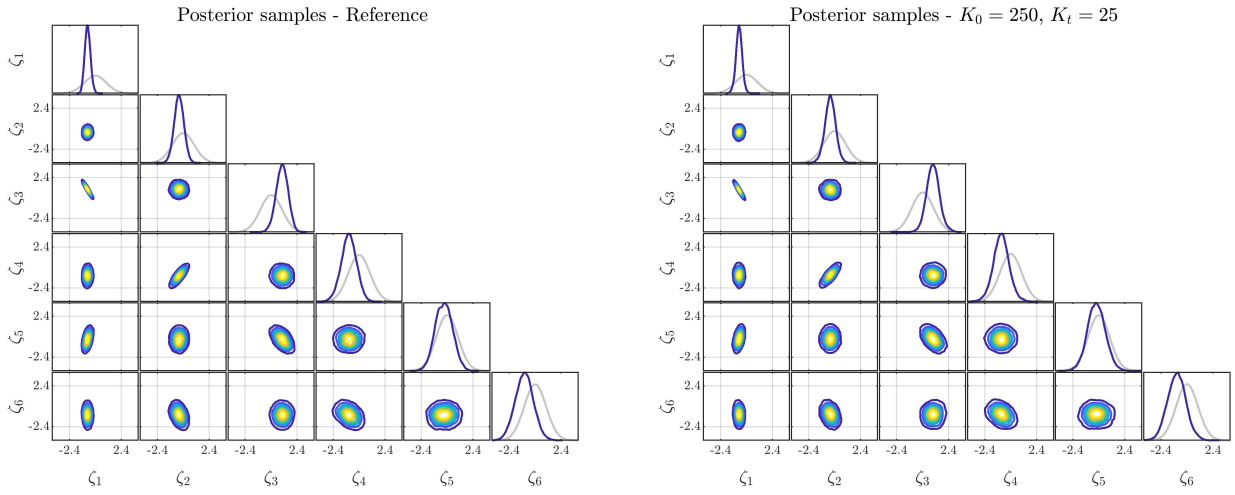

(a) Reference

(b) $K_0 = 250$, $K_t/K_0 = 0.1$

Figure 13: Diffusion problem: posterior univariate and bivariate marginal PDF of the six first KL eigenmodes

$\sqrt{\mathbf{Var}[\zeta_i \vert \boldsymbol{d}]}$	K_0	K_t/K_0	$\mathbb{E}[N_c]$	ζ_1	ζ_2	ζ_3	ζ_4	ζ_5	ζ_6
BUS-PCK	100	0.1	127	0.45 (69.5)	0.71 (59.0)	0.87 (59.1)	0.98 (38.9)	1.13 (43.2)	1.07 (28.0)
	100	0.2	159.6	0.38 (44.5)	0.62 (40.3)	0.77 (39.6)	0.86 (22.8)	1.00 (26.6)	1.04 (24.1)
	250	0.1	342.5	0.29 (8.9)	0.49 (10.7)	0.60 (9.1)	0.74 (4.8)	0.82 (3.9)	0.84 (0.7)
	250	0.2	449	0.28 (5.5)	0.48 (7.1)	0.58 (6.3)	0.72 (2.7)	0.81 (3.3)	0.85 (1.3)
	500	0.1	730	0.26 (0.2)	0.45 (1.4)	0.55 (0.2)	0.69 (1.3)	0.79 (0.2)	0.85 (1.8)
	500	0.2	968	0.26 (0.4)	0.45 (0.4)	0.55 (0.3)	0.70 (1.0)	0.77 (2.1)	0.83 (0.4)
Reference			**27600**	**0.26**	**0.44**	**0.55**	**0.70**	**0.79**	**0.84**

Table 6: Diffusion problem: posterior standard deviations of few KL eigenmodes.

	K_0	K_t/K_0	$\mathbb{E}[N_c]$	$\mathcal{Z}$
BUS-PCK	100	0.1	127	87.09 (254.1)
	100	0.2	159.6	29.41 (19.6)
	250	0.1	342.5	22.73 (7.6)
	250	0.2	449	23.36 (5.0)
	500	0.1	730	23.75 (3.4)
	500	0.2	968	24.77 (0.7)
Reference			**27600**	**24.59**

Table 7: Diffusion problem: model evidence values.

Next, a comparison between the true log-diffusivity field, the reference posterior log-diffusivity field and that obtained with the proposed approach for $K_0 \in \{250, 500\}$ and $\kappa = 0.2$ is given in Fig. 14. As a validation of the reference results, one observes that the posterior log-diffusivity field obtained from SuS procedure matches well with the realization used for generating the synthetic data. Furthermore, the proposed approach provides a fair approximation of the posterior log-diffusivity when $K_0 = 250$ and $\kappa = 0.2$, with a slight overestimation of the variance, though (see Fig.14a). Then, the posterior log-diffusivity field is well approximated when $K_0 = 500$ and $\kappa = 0.2$ (see Fig. 14b).

Then, contours of the reference posterior covariance kernel of the log-diffusivity field and its approximations

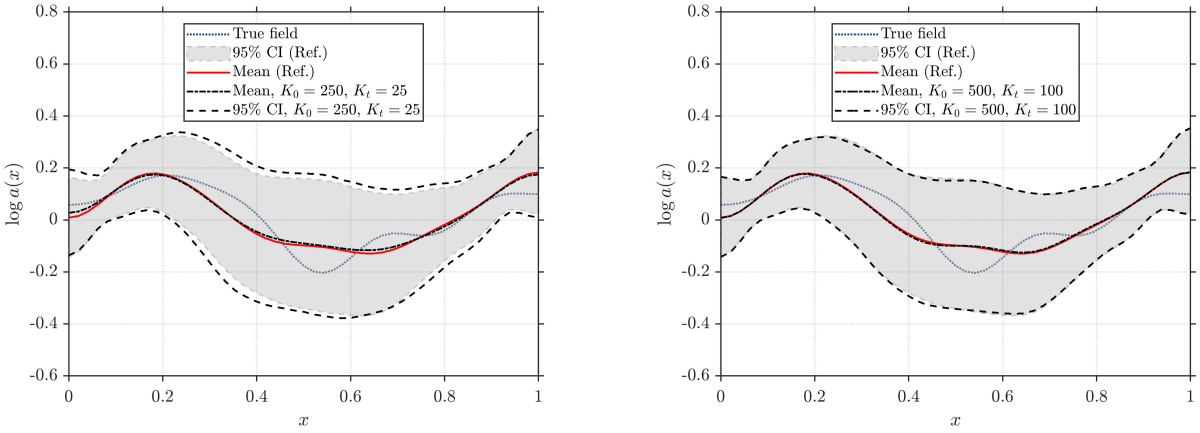

(a) $K_0 = 250$, $K_t/K_0 = 0.2$ (b) $K_0 = 500$, $K_t/K_0 = 0.2$

Figure 14: Diffusion problem: posterior log-diffusivity field.

provided by the proposed approach for $K_0 \in \{250, 500\}$ and $\kappa = 0.2$ are shown in Fig. 15. Approximately 450 model calls are sufficient to provide a quite accurate approximation of the covariance kernel, in its positive correlation zones (see Fig.15a). The case $K_0 = 500$ and $\kappa = 0.2$ presents a sensibly accurate approximation of the posterior covariance kernel, even in the zones which exhibit negative correlations (see Fig.15b).

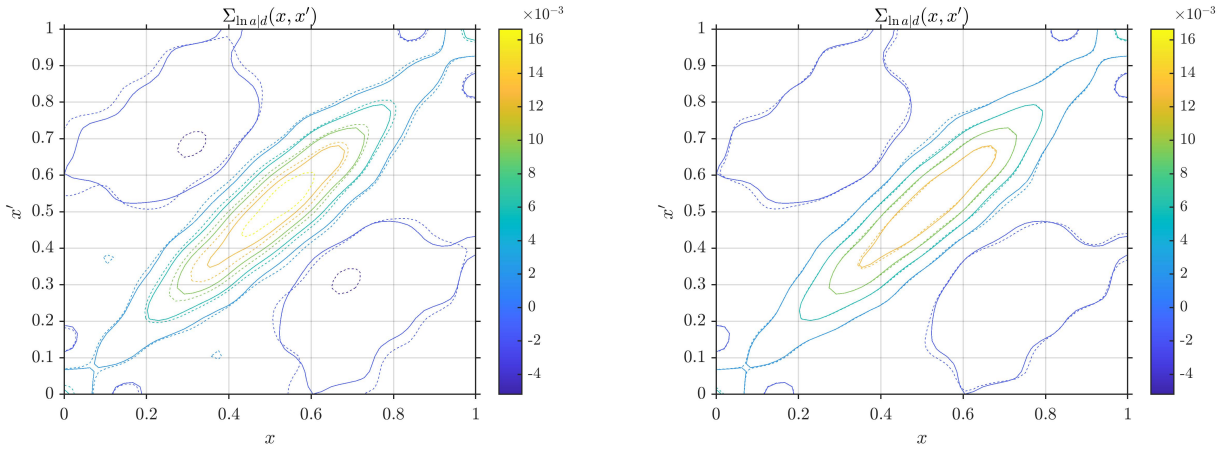

(a) $K_0 = 250$, $K_t/K_0 = 0.2$ (b) $K_0 = 500$, $K_t/K_0 = 0.2$

Figure 15: Diffusion problem: posterior covariance kernel of the log-diffusivity field. Continuous lines refer to reference results, whereas dashed lines refer to ones provided by the proposed approach.

Lastly, it is worth noting that a satisfactory approximation of the posterior PDF is obtained with an average number of model calls of $\mathbb{E}[N_c] = 730$, which represents a reduction of about 97.4% of the total cost of $2.76 \cdot 10^4$ required by an inversion using the full likelihood (see Tab. 5 & 6).

6. Conclusion

In this paper, a Bayesian inversion method using adaptive surrogate models has been presented, based on the BUS framework [25, 26], which aims at reformulating the classical Bayesian inference into the estimation of

a rare event. In this framework, the method combines a well-known Structural Reliability (SR) method known as Subset Simulation (SuS) [29, 30] and adaptive Polynomial Chaos Kriging (PCK) [42, 43], which provides powerful surrogate models able to approximate both global and local behaviors of computational models. In this context, a PCK surrogate model is firstly built in order to catch the global trend of the log-likelihood on the prior support. This surrogate model is subsequently enriched throughout the SuS sampling procedure by selecting points in informative regions, based on principles taken from active learning SR methods [39, 78, 41]. The Kriging part of the surrogate model then enables to better catch local variations of log-likelihood, as well as provide an local error measure which can be used for enriching the surrogate model.

The proposed approach has been applied to three cases studies of increasing complexity, involving a one-dimensional analytical function, a two degrees-of-freedom structure and a diffusion problem with moderate active dimensionality. It appears from numerical investigations that the proposed approach provides accurate approximations of the posterior distributions, even in the case of likelihood functions with localized behavior, or multi-modal distributions, which are usually difficult to sample for many existing Bayesian inversion algorithms. Moreover, such approximations have been obtained for a quite limited amount of model calls (*i.e.* $\approx 50 - 500$), which makes the proposed approach suitable for computationally demanding models. For each test case studied, the proposed approach has provided a reduction of at least 97.5% of the total number of model calls required by aBUS-SuS inversions using the full likelihood function. Furthermore, classical MCMC-based Bayesian inversion approaches do not enable to assess the performance of several models against observed data, since the computation of the model evidence is avoided [6]. A particular advantage provided by the BUS framework is that the proposed approach enables to estimate the model evidence, as a by-product of the rare event estimation through the SuS procedure. Therefore, the proposed method would be suitable for model selection [88].

Then, the proposed approach presents several shortcomings, which may be addressed in further works. Firstly, the updating step of the BUS scaling constant is based on the computation of the convex hull of the current experimental design of the PCK surrogate model, in order to filter points whose surrogate model predictions are too uncertain. This is done for limiting the risk of making a wrong estimation of the maximal likelihood value needed for updating the BUS scaling constant. As mentioned in [75], the Quickhull algorithm [76] used for computing convex hulls significantly suffers from the so-called *curse of dimensionality*. Indeed, for dimensions larger than ≈ 15, the number of facets of the computed convex hull grows fast with dimension, which considerably slows the overall procedure. Then, it would be necessary to define an alternative filter for updating the BUS scaling constant, based on the distance to the current points of experimental design, and the uncertainties associated to predictions of likelihood values. Moreover, the optimization problem involved in the training of Kriging parameters may be difficult to solve in high dimensions [75, 38]. This is in line with results from a recent survey and benchmark on surrogate-based active learning SR methods [84], which suggest that PCK surrogate models are well suited for parameter dimensions $d < 20$, whereas PCE surrogates perform well in higher dimensions $d \geq 20$. Thus, the proposed approach may be adapted to PCE for tackling problems with higher dimensions, provided a local error estimate adapted to PCE is used. In this context, the Fraction of Boostrap Replicates (FBR) introduced in [73] could be used in the framework of the proposed adaptive point

enrichment scheme. Such guidelines might be considered in further work for tackling problems with higher dimensions. Lastly, it appears from test cases results that the stopping criterion of the point enrichment step has been rarely reached during calculations. This may be due to the fact that the adopted threshold value for the misclassification probability (see Section 4.3) is too conservative, as underlined in [41]. Therefore, a more precise stopping criterion may be defined in order to avoid unnecessary model calls throughout the Bayesian updating scheme.

References

[1] J. Kaipio, E. Somersalo, Statistical and Computational Inverse Problems, Springer, 2005. doi:10.1007/b138659.
URL http://dx.doi.org/10.1007/b138659

[2] J. Idier, Bayesian Approach to Inverse Problems, ISTE, 2008. doi:10.1002/9780470611197.
URL http://dx.doi.org/10.1002/9780470611197

[3] A. M. Stuart, Inverse problems : a Bayesian perspective, Acta Numer. 19 (2010) 451–559. doi:10.1017/s0962492910000061.

[4] G. Claeskens, N. L. Hjort, Model Selection and Model Averaging, Cambridge Series in Statistical and Probabilistic Mathematics, Cambridge University Press, 2008. doi:10.1017/CBO9780511790485.

[5] C. P. Robert, G. Casella, Monte Carlo Statistical Methods, 2nd Edition, Springer Series in Statistics, New York, 2004. doi:10.1007/978-1-4757-4145-2.

[6] S. Brooks, A. Gelman, G. Jones, X.-L. Meng, Handbook of Markov Chain Monte Carlo, Chapman & Hall/CRC, Boca Raton, Florida, USA, 2011. doi:10.1201/b10905.

[7] N. Metropolis, A. W. Rosenbluth, A. H. Teller, Equations of state calculations by fast computing machines, J. Chem. Phys. 21 (1953) 1087–1092. doi:10.2172/4390578.

[8] W. Hastings, Monte Carlo sampling methods using Markov chains and their application, Biometrika 57 (1970) 97–109. doi:10.1093/biomet/57.1.97.

[9] H. Haario, M. Laine, A. Mira, E. Saksman, DRAM: Efficient adaptive MCMC, Statistics and Computing 16 (4) (2006) 339–354. doi:10.1007/s11222-006-9438-0.
URL https://doi.org/10.1007/s11222-006-9438-0

[10] C. Andrieu, J. Thoms, A tutorial on adaptive MCMC, Statistics and Computing 18 (4) (2008) 343–373. doi:10.1007/s11222-008-9110-y.
URL https://doi.org/10.1007/s11222-008-9110-y

[11] R. M. Neal, MCMC Using Hamiltonian Dynamics, Chapman & Hall - CRC Press, Boca Raton London, 2011, Ch. 5, p. 13–162.

[12] J. Goodman, J. Weare, Ensemble samplers with affine invariance, Commun. Appl. Math. Comput. Sci. 5 (1) (2010) 65–80. doi:10.2140/camcos.2010.5.65.
URL https://doi.org/10.2140/camcos.2010.5.65

[13] M. Cowles, B. Carlin, Markov chain Monte Carlo convergence diagnostics : a comparative review, J. Amer. Stat. Assoc. 91 (1996) 883–904. doi:10.1080/01621459.1996.10476956.

[14] S. E. Adlouni, A. Favre, B. Bobée, Comparison of methodologies to assess the convergence of Markov chain Monte Carlo methods, Computational Statistics & Data Analysis 50 (2006) 2685–2701. doi:10.1016/j.csda.2005.04.018.

[15] A. Gelman, B. Rubin, Inference from iterative simulation using multiple sequences, Statistical Science 7 (1992) 457–472. doi:10.1214/ss/1177011136.

[16] C. W. Fox, S. J. Roberts, A tutorial on variational Bayesian inference, Artificial Intelligence Review 38 (2) (2012) 85–95. doi:10.1007/s10462-011-9236-8.
URL https://doi.org/10.1007/s10462-011-9236-8

[17] J.-M. Marin, P. Pudlo, C. P. Robert, R. J. Ryder, Approximate Bayesian computational methods, Statistics and Computing 22 (6) (2012) 1167–1180. doi:10.1007/s11222-011-9288-2.
URL https://doi.org/10.1007/s11222-011-9288-2

[18] L. Tierney, R. E. Kass, J. B. Kadane, Approximate Marginal Densities of Nonlinear Functions, Biometrika 76 (3) (1989) 425–433. doi:10.2307/2336109.
URL http://www.jstor.org/stable/2336109

[19] J. Skilling, Nested Sampling for General Bayesian Computation, Bayesian Analysis 1 (4) (2006) 833–860. doi:10.1214/06-ba127.

[20] A. H. Elsheikh, M. F. Wheeler, I. Hoteit, Hybrid nested sampling algorithm for Bayesian model selection applied to inverse subsurface flow problems, Journal of Computational Physics 258 (2014) 319–337. doi:https://doi.org/10.1016/j.jcp.2013.10.001.
URL https://www.sciencedirect.com/science/article/pii/S0021999113006669

[21] T. El Moselhy, Y. Marzouk, Bayesian inference with optimal maps, Journal of Computational Physics 231 (23) (2012) 7815–7850. doi:10.1016/j.jcp.2012.07.022.

[22] J. B. Nagel, B. Sudret, Spectral likelihood expansions for Bayesian inference, Journal of Computational Physics 309 (2016) 267–294. doi:10.1016/j.jcp.2015.12.047.

[23] P.-R. Wagner, S. Marelli, B. Sudret, Bayesian model inversion using stochastic spectral embedding, Journal of Computational Physics 436 (2021) 110141. doi:https://doi.org/10.1016/j.jcp.2021.110141.
URL https://www.sciencedirect.com/science/article/pii/S0021999121000334

[24] S. Marelli, P.-R. Wagner, C. Lataniotis, B. Sudret, Stochastic Spectral Embedding, International Journal for Uncertainty Quantification 11 (2) (2021) 25–47. doi:10.1615/Int.J.UncertaintyQuantification.2020034395.

[25] D. Straub, I. Papaioannou, Bayesian Updating with Structural Reliability Methods, Journal of Engineering Mechanics 141 (3) (2015) 04014134. doi:10.1061/(ASCE)EM.1943-7889.0000839.

[26] D. Straub, I. Papaioannou, W. Betz, Bayesian analysis of rare events, Journal of Computational Physics 314 (2016) 538–556. doi:https://doi.org/10.1016/j.jcp.2016.03.018.
URL https://www.sciencedirect.com/science/article/pii/S0021999116001704

[27] R. Rackwitz, B. Flessler, Structural reliability under combined random load sequences, Computers & Structures 9 (5) (1978) 489–494. doi:https://doi.org/10.1016/0045-7949(78)90046-9.
URL https://www.sciencedirect.com/science/article/pii/0045794978900469

[28] R. E. Melchers, A. T. Beck, Structural reliability analysis and prediction, John Wiley & Sons Ltd, Hoboken, NJ, 2018. doi:10.1002/9781119266105.

[29] S.-K. Au, J. L. Beck, Estimation of small failure probabilities in high dimensions by subset simulation, Probabilistic Engineering Mechanics 16 (4) (2001) 263–277. doi:https://doi.org/10.1016/S0266-8920(01)00019-4.
URL https://www.sciencedirect.com/science/article/pii/S0266892001000194

[30] W. Betz, I. Papaioannou, J. L. Beck, D. Straub, Bayesian inference with Subset Simulation: Strategies and improvements, Computer Methods in Applied Mechanics and Engineering 331 (2018) 72–93. doi:https://doi.org/10.1016/j.cma.2017.11.021.
URL https://www.sciencedirect.com/science/article/pii/S0045782517307211

[31] Y. M. Marzouk, H. N. Najm, L. A. Rahn, Stochastic spectral methods for efficient Bayesian solution of inverse problems, Journal of Computational Physics 224 (2) (2007) 560–586. doi:10.1016/j.jcp.2006.10.010.

[32] Y. M. Marzouk, D. B. Xiu, A stochastic collocation approach to Bayesian inference in inverse problems, Commun. Comput. Phys. 6 (2009) 826–847. doi:10.4208/cicp.2009.v6.p826.

[33] Y. M. Marzouk, H. N. Najm, Dimensionality reduction and polynomial chaos acceleration of Bayesian inference in inverse problems, Journal of Computational Physics 228 (6) (2009) 1862–1902. doi:10.1016/j.jcp.2008.11.024.

[34] A. M. Stuart, A. L. Teckentrup, Posterior consistency for Gaussian process approximations of Bayesian posterior distributions, Mathematics of Computation 87 (310) (2017) 721–753. doi:10.1090/mcom/3244.
URL http://dx.doi.org/10.1090/mcom/3244

[35] L. Yan, T. Zhou, Adaptive multi-fidelity polynomial chaos approach to Bayesian inference in inverse problems, Journal of Computational Physics 381 (2019) 110–128. doi:https://doi.org/10.1016/j.jcp.2018.12.025.
URL https://www.sciencedirect.com/science/article/pii/S0021999119300063

[36] L. Yan, T. Zhou, An Adaptive Surrogate Modeling Based on Deep Neural Networks for Large-Scale Bayesian Inverse Problems, Communications in Computational Physics 28 (5) (2020) 2180–2205. doi:https://doi.org/10.4208/cicp.OA-2020-0186.
URL http://global-sci.org/intro/article_detail/cicp/18409.html

[37] D. G. Giovanis, I. Papaioannou, D. Straub, V. Papadopoulos, Bayesian updating with subset simulation using artificial neural networks, Computer Methods in Applied Mechanics and Engineering 319 (2017) 124–145. doi:https://doi.org/10.1016/j.cma.2017.02.025.
URL https://www.sciencedirect.com/science/article/pii/S0045782516311914

[38] Z. Wang, A. Shafieezadeh, Highly efficient Bayesian updating using metamodels: An adaptive Kriging-based approach, Structural Safety 84 (2020) 101915. doi:https://doi.org/10.1016/j.strusafe.2019.101915.
URL https://www.sciencedirect.com/science/article/pii/S0167473019303790

[39] B. Echard, N. Gayton, M. Lemaire, AK-MCS: An active learning reliability method combining Kriging and Monte Carlo Simulation, Structural Safety 33 (2) (2011) 145–154. doi:https://doi.org/10.1016/j.strusafe.2011.01.002.
URL https://www.sciencedirect.com/science/article/pii/S0167473011000038

[40] R. Teixeira, M. Nogal, A. O'Connor, Adaptive approaches in metamodel-based reliability analysis: A review, Structural Safety 89 (2021) 102019. doi:https://doi.org/10.1016/j.strusafe.2020.102019.
URL https://www.sciencedirect.com/science/article/pii/S0167473020300989

[41] F. Cui, M. Ghosn, Implementation of machine learning techniques into the Subset Simulation method, Structural Safety 79 (2019) 12–25. doi:https://doi.org/10.1016/j.strusafe.2019.02.002.
URL https://www.sciencedirect.com/science/article/pii/S0167473018301759

[42] R. Schöbi, B. Sudret, J. Wiart, Polynomial chaos based Kriging, International Journal for Uncertainty Quantification 5 (2) (2015) 171–193. doi:10.1615/int.j.uncertaintyquantification.2015012467.
URL http://dx.doi.org/10.1615/Int.J.UncertaintyQuantification.2015012467

[43] R. Schöbi, B. Sudret, S. Marelli, Rare Event Estimation Using Polynomial-Chaos Kriging, ASCE-ASME Journal of Risk and Uncertainty in Engineering Systems, Part A: Civil Engineering 3 (2). doi:10.1061/ajrua6.0000870.
URL http://dx.doi.org/10.1061/AJRUA6.0000870

[44] F. Lu, M. Morzfeld, X. Tu, A. J. Chorin, Limitations of polynomial chaos expansions in the bayesian solution of inverse problems, Journal of Computational Physics 282 (2015) 138–147. doi:10.1016/j.jcp.2014.11.010.

[45] M. J. Zaki, W. Meira, Jr, Data Mining and Analysis: Fundamental Concepts and Algorithms, Cambridge University Press, 2014. doi:10.1017/CBO9780511810114.

[46] O. Ditlevsen, H. Madsen, Structural reliability methods, J. Wiley and Sons, Chichester, 1996.

[47] M. Lemaire, Structural reliability, Wiley, 2009.

[48] K. M. Zuev, J. L. Beck, S.-K. Au, L. S. Katafygiotis, Bayesian post-processor and other enhancements of Subset Simulation for estimating failure probabilities in high dimensions, Computers & Structures 92-93 (2012) 283–296. doi:https://doi.org/10.1016/j.compstruc.2011.10.017.
URL https://www.sciencedirect.com/science/article/pii/S0045794911002720

[49] I. Papaioannou, W. Betz, K. Zwirglmaier, D. Straub, MCMC algorithms for Subset Simulation, Probabilistic Engineering Mechanics 41 (2015) 89–103. doi:https://doi.org/10.1016/j.probengmech.2015.06.006.
URL https://www.sciencedirect.com/science/article/pii/S0266892015300205

[50] A. Nataf, Détermination des distributions dont les marges sont données, C. R. Acad. Sci. 225 (1962) 42–43.

[51] R. Lebrun, A. Dutfoy, An innovating analysis of the Nataf transformation from the copula viewpoint, Probabilistic Engineering Mechanics 24 (3) (2009) 312–320. doi:https://doi.org/10.1016/j.probengmech.2008.08.001.
URL https://www.sciencedirect.com/science/article/pii/S0266892008000660

[52] M. Rosenblatt, Remarks on a Multivariate Transformation, The Annals of Mathematical Statistics 23 (3) (1952) 470 – 472. doi:10.1214/aoms/1177729394.
URL https://doi.org/10.1214/aoms/1177729394

[53] W. Betz, J. L. Beck, I. Papaioannou, D. Straub, Bayesian inference with reliability methods without knowing the maximum of the likelihood function, Probabilistic Engineering Mechanics 53 (2018) 14–22. doi:https://doi.org/10.1016/j.probengmech.2018.03.004.
URL https://www.sciencedirect.com/science/article/pii/S026689201730190X

[54] F. DiazDelaO, A. Garbuno-Inigo, S. Au, I. Yoshida, Bayesian updating and model class selection with Subset Simulation, Computer Methods in Applied Mechanics and Engineering 317 (2017) 1102–1121. doi:https://doi.org/10.1016/j.cma.2017.01.006.
URL https://www.sciencedirect.com/science/article/pii/S0045782516308283

[55] G. Blatman, B. Sudret, An adaptive algorithm to build up sparse polynomial chaos expansions for stochastic finite element analysis, Prob. Eng. Mech. 25 (2010) 183–197. doi:10.1016/j.probengmech.2009.10.003.

[56] J. D. Jakeman, F. Franzelin, A. Narayan, M. Eldred, D. Plfüger, Polynomial chaos expansions for dependent random variables, Computer Methods in Applied Mechanics and Engineering 351 (2019) 643 – 666. doi:https://doi.org/10.1016/j.cma.2019.03.049.
URL http://www.sciencedirect.com/science/article/pii/S0045782519301884

[57] R. Ghanem, P. Spanos, Stochastic finite elements - A spectral approach, Springer Verlag, 1991. doi:10.1007/978-1-4612-3094-6.

[58] D. Xiu, G. E. Karniadakis, The Wiener-Askey Polynomial Chaos for Stochastic Differential Equations, SIAM Journal on Scientific Computing 24 (2002) 619–644. doi:10.1137/S1064827501387826.

[59] N. Wiener, The homogeneous chaos, Am. J. Math. 60 (1938) 897–936. doi:10.2307/2371268.

[60] C. Soize, R. Ghanem, Physical Systems with Random Uncertainties: Chaos Representations with Arbitrary Probability Measure, SIAM Journal on Scientific Computing 26 (2) (2004) 395–410. doi:10.1137/s1064827503424505.
URL http://dx.doi.org/10.1137/S1064827503424505

[61] O. G. Ernst, A. Mugler, H.-J. Starkloff, E. Ullmann, On the convergence of generalized polynomial chaos expansions, ESAIM: Mathematical Modelling and Numerical Analysis 46 (2) (2012) 317–339. doi:10.1051/m2an/2011045.
URL https://www.esaim-m2an.org/articles/m2an/abs/2012/02/m2an110045/m2an110045.html

[62] D. Ghiocel, R. Ghanem, Stochastic finite element analysis of seismic soil-structure interaction, Journal of Engineering Mechanics 128 (2002) 66–77. doi:10.1061/(asce)0733-9399(2002)128:1(66).

[63] O. P. Le Maître, M. T. Reagan, H. N. Najm, R. G. Ghanem, O. M. Knio, A Stochastic Projection Method for Fluid Flow: II. Random Process, Journal of Computational Physics 181 (1) (2002) 9 – 44. doi:https://doi.org/10.1006/jcph.2002.7104.
URL http://www.sciencedirect.com/science/article/pii/S0021999102971044

[64] D. Xiu, Efficient Collocational Approach for Parametric Uncertainty Analysis, Communications in Computational Physics 2 (2) (2007) 293–309.

[65] S.-K. Choi, R. V. Grandhi, R. A. Canfield, C. L. Pettit, Polynomial Chaos Expansion with Latin Hypercube Sampling for Estimating Response Variability, AIAA Journal 42 (6) (2004) 1191–1198. arXiv:https://doi.org/10.2514/1.2220, doi:10.2514/1.2220.
URL https://doi.org/10.2514/1.2220

[66] M. Berveiller, B. Sudret, M. Lemaire, Stochastic finite element: a non intrusive approach by regression, European Journal of Computational Mechanics 15 (1-3) (2006) 81–92. arXiv:https://doi.org/10.3166/remn.15.81-92, doi:10.3166/remn.15.81-92.
URL https://doi.org/10.3166/remn.15.81-92

[67] G. Blatman, B. Sudret, Adaptive sparse polynomial chaos expansion based on Least Angle Regression, J. Comput. Phys. 230 (2011) 2345–2367. doi:10.1016/j.jcp.2010.12.021.

[68] D. Donoho, Compressed sensing, IEEE Transactions on Information Theory 52 (4) (2006) 1289–1306. doi:10.1109/TIT.2006.871582.

[69] N. Lüthen, S. Marelli, B. Sudret, Sparse Polynomial Chaos Expansions: Literature Survey and Benchmark, SIAM/ASA Journal on Uncertainty Quantification 9 (2) (2021) 593–649. doi:10.1137/20m1315774.
URL http://dx.doi.org/10.1137/20M1315774

[70] S. Arlot, A. Celisse, A survey of cross-validation procedures for model selection, Statistics Surveys 4 (2010) 40–79. doi:10.1214/09-ss054.

[71] T. J. Santner, B. J. Williams, W. I. Notz, The Design and Analysis of Computer Experiments, Springer New York, 2003. doi:10.1007/978-1-4757-3799-8.
URL http://dx.doi.org/10.1007/978-1-4757-3799-8

[72] O. Dubrule, Cross validation of kriging in a unique neighborhood, Journal of the International Association for Mathematical Geology 15 (6) (1983) 687–699. doi:10.1007/BF01033232.
URL https://doi.org/10.1007/BF01033232

[73] S. Marelli, B. Sudret, An active-learning algorithm that combines sparse polynomial chaos expansions and bootstrap for structural reliability analysis, Structural Safety 75 (2018) 67–74. doi:https://doi.org/10.1016/j.strusafe.2018.06.003.
URL https://www.sciencedirect.com/science/article/pii/S0167473017302977

[74] V. Dubourg, Adaptive surrogate models for reliability analysis and reliability-based design optimization, Ph.D. thesis, Univertisté Clermont-Ferrand 2 (2011).
URL http://www.theses.fr/2011CLF22184

[75] P. Angelikopoulos, C. Papadimitriou, P. Koumoutsakos, X-TMCMC: Adaptive kriging for Bayesian inverse modeling, Computer Methods in Applied Mechanics and Engineering 289 (2015) 409–428. doi:https://doi.org/10.1016/j.cma.2015.01.015.
URL https://www.sciencedirect.com/science/article/pii/S0045782515000353

[76] C. B. Barber, D. P. Dobkin, H. Huhdanpaa, The Quickhull Algorithm for Convex Hulls, ACM Trans. Math. Softw. 22 (4) (1996) 469–483. doi:10.1145/235815.235821.
URL https://doi.org/10.1145/235815.235821

[77] B. J. Bichon, M. S. Eldred, L. P. Swiler, S. Mahadevan, J. M. McFarland, Efficient Global Reliability Analysis for Nonlinear Implicit Performance Functions, AIAA Journal 46 (10) (2008) 2459–2468. arXiv:https://doi.org/10.2514/1.34321, doi:10.2514/1.34321.
URL https://doi.org/10.2514/1.34321

[78] M. Moustapha, B. Sudret, Surrogate-assisted reliability-based design optimization: a survey and a unified modular framework, Structural and Multidisciplinary Optimization 60 (5) (2019) 2157–2176. doi:10.1007/s00158-019-02290-y.
URL https://doi.org/10.1007/s00158-019-02290-y

[79] J. Bect, D. Ginsbourger, L. Li, V. Picheny, E. Vazquez, Sequential design of computer experiments for the estimation of a probability of failure, Statistics and Computing 22 (3) (2011) 773–793. doi:10.1007/s11222-011-9241-4.
URL http://dx.doi.org/10.1007/s11222-011-9241-4

[80] R. Teixeira, M. Nogal, A. O'Connor, B. Martinez-Pastor, Reliability assessment with density scanned adaptive Kriging, Reliability Engineering & System Safety 199 (2020) 106908. doi:https://doi.org/10.1016/j.ress.2020.106908.
URL https://www.sciencedirect.com/science/article/pii/S0951832019307434

[81] S. Marelli, B. Sudret, UQLab: A framework for uncertainty quantification in Matlab, in: Proc. 2nd Int. Conf. onVulnerability, Risk Analysis and Management (ICVRAM2014), Liverpool, United Kingdom, 2014, pp. 2554–2563.

[82] S. Kullback, R. Leibler, On information and sufficiency, Annals of Mathematical Statistics 22 (1951) 79–86. doi:10.1214/aoms/1177729694.

[83] J. Lin, Divergence measures based on the Shannon entropy, IEEE Transactions on Information Theory 37 (1) (1991) 145–151. doi:10.1109/18.61115.

[84] M. Moustapha, S. Marelli, B. Sudret, A generalized framework for active learning reliability: survey and benchmark, arXiv:2106.01713 [stat]ArXiv: 2106.01713.
URL http://arxiv.org/abs/2106.01713

[85] J. L. Beck, S.-K. Au, Bayesian Updating of Structural Models and Reliability using Markov Chain Monte Carlo Simulation, Journal of Engineering Mechanics 128 (4) (2002) 380–391. doi:10.1061/(ASCE)0733-9399(2002)128:4(380).

[86] J. L. Beck, K. M. Zuev, Asymptotically independent Markov sampling: a new Markov Chain Monte Carlo scheme for Bayesian inference, International Journal for Uncertainty Quantification 3 (5) (2013) 445–474. doi:10.1615/Int.J.UncertaintyQuantification.2012004713.

[87] M. Loève, Probability theory, Springer Verlag, 1977. doi:10.1007/978-1-4757-6288-4.

[88] J. L. Beck, K.-V. Yuen, Model Selection Using Response Measurements: Bayesian Probabilistic Approach, Journal of Engineering Mechanics 130 (2) (2004) 192–203. doi:10.1061/(ASCE)0733-9399(2004)130:2(192).